# Final Scientific/Technical Report

February 2012


*Project Title*: A closed path methane and water vapor gas analyzer.

# Final Scientific/Technical Report

*Project Title*: A closed path methane and water vapor gas analyzer.

| | |
|---|---|
| *Principle Investigator:* | Dr. Liukang Xu |
| *Business Officer:* | Dayle K. McDermitt |
| *Project Manager:* | Derek Trutna |
| *Topic Number/Subtopic Letter:* | 16-b |
| *Company Name:* | LI-COR Biosciences |
| *Address:* | 4647 Superior Street<br>Lincoln, Nebraska 68504 USA |
| *Website:* | http://www.licor.com |
| *Telephone:* | 402-467-3576<br>800-447-3576 |
| *Fax*: | 402-467-2819 |

Founded in 1971, LI-COR Biosciences is a leader in the design and manufacturer of instrument systems for environmental and biotechnology research. LI-COR Biosciences instruments for photosynthesis, carbon dioxide analysis and light measurement are recognized worldwide for standard-setting innovation in plant science research and environmental monitoring. LI-COR also is a pioneer in the development of infrared fluorescence labeling and detection systems for such areas as drug discovery and DNA sequencing for genomic research.

LI-COR instruments are used in over 100 countries and are supported by a global network of distributors. The company is based in Lincoln, Nebraska, with subsidiaries in Germany and the United Kingdom.

## SBIR/STTR Rights Notice

SBIR/STTR data is furnished with SBIR/STTR rights under Grant No. DE-FG02-08ER84968 (and subcontractor non if appropriate). For a period of four years after acceptance of all items to be delivered under this grant, the Government agrees to use this data for Government purposes only and information enclosed should not be disclosed outside the Government (including disclosure for procurement purposes) during such period without permission of the grantee, except that, subject to the foregoing use and disclosure prohibits, such data may be disclosed for use by support contractors. After the aforesaid four-year period, the Government has a royalty-free license to use, and to authorize others to use on its behalf, this data for Government purposes, but is relieved of all disclosure prohibitions and assumes no liability for unauthorized use of this data by third parties. This Notice shall be affixed to any reproduction of this data in whole or in part.

(**End of Notice**)

# Table of Contents

# 1.0 Project Summary

Robust, economical, low-power and reliable closed-path methane ($CH_4$), carbon dioxide ($CO_2$), and water vapor ($H_2O$) analyzers suitable for long-term measurements are not readily available commercially. Such analyzers are essential for quantifying the amount of $CH_4$ and $CO_2$ released from various ecosystems (wetlands, rice paddies, forests, etc.) and other surface contexts (e.g. landfills, animal husbandry lots, etc.), and for understanding the dynamics of the atmospheric $CH_4$ and $CO_2$ budget and their impact on climate change and global warming.

The purpose of this project is to develop a closed-path methane, carbon dioxide gas and water vapor analyzer capable of long-term measurements in remote areas for global climate change and environmental research. The analyzer will be capable of being deployed over a wide range of ecosystems to understand methane and carbon dioxide exchange between the atmosphere and the surface. Measurements of methane and carbon dioxide exchange need to be made all year-round with limited maintenance requirements.

During this Phase II effort, we successfully completed the design of the electronics, optical bench, trace gas detection method and mechanical infrastructure. We are using the technologies of two vertical cavity surface emitting lasers, a multiple-pass Herriott optical cell, wavelength modulation spectroscopy and direct absorption to measure methane, carbon dioxide, and water vapor. We also have designed the instrument application software, Field Programmable Gate Array (FPGA), along with partial completion of the embedded software. The optical bench has been tested in a lab setting with very good results. Major sources of optical noise have been identified and through design, the optical noise floor is approaching -60dB. Both laser modules can be temperature controlled to help maximize the stability of the analyzer. Additionally, a piezo electric transducer has been utilized to randomize the noise introduced from potential etalons. It is expected that all original specifications contained within the initial proposal will be met.

We are currently in the beginning stages of assembling the first generation prototypes and finalizing the remaining design elements. The first prototypes will initially be tested in our environmental calibration chamber in which specific gas concentrations, temperature and humidity levels can be controlled. Once operation in this controlled setting is verified, the prototypes will be deployed at LI-COR's Experimental Research Station (LERS). Deployment at the LERS site will test the instrument's robustness in a real-world situation.

## 2.0 Introduction

LI-COR was awarded both the Phase I and Phase II grants to develop a tunable diode laser-based, closed-path methane and water vapor analyzer using a wavelength modulation spectroscopy (WMS) approach and a vertical cavity surface emitting laser (VCSEL) at 1.651 µm. The proposed analyzer will also have the capability to measure temperature, pressure, and water vapor concentration *in situ* at a sufficient accuracy for dilution and band broadening corrections, so the analyzer can output dry mole fraction of methane. During our initial design, we realized the importance of simultaneously measuring methane and carbon dioxide and have since added the measurement of carbon dioxide to the scope of this project.

Topic 16-b of FY2008 DOE SBIR Phase I program seeks proposals, "to develop new technology platform that can be used to measure fluxes and/or concentrations of important trace gas constitutes in the atmosphere, such as isotopes of carbon, methane, CO, etc. New instrumentation designs must have high potential for direct application for determining carbon, CO and trace species sources and sinks. Also, design elements that ensure long-term and robust field deployment, should be included."

Methane plays critical roles in the radiation balance and chemistry of the atmosphere. According to studies reported in the literature (e.g. Rodhe, 1990; Hansen and Sato, 2001) and the most recently published IPCC Fourth Assessment Report (IPCC, 2007), methane is the second most important greenhouse gas after carbon dioxide, and currently contributes 0.48 W $m^{-2}$ to anthropogenic radiative forcing compared with 1.66 W $m^{-2}$ from $CO_2$. Several studies have demonstrated that $CH_4$ deserves greater attention and should be considered separately from $CO_2$ when considering the impact of greenhouse gases on climate forcing (e.g. Hansen and Sato, 2001), even though $CH_4$ and $CO_2$ are intimately linked in the global carbon cycle. In addition to climate forcing, the increase in atmospheric methane has contributed to approximately half the estimated increase in global tropospheric ozone (Ehhalt and Prather, 2001), which has a negative impact on the health of living organisms.

The globally-averaged atmospheric methane concentration has increased from a pre-industrial level of about 715 ppb (Etheridge et al., 1998) to 1775 ppb in 2005 (Dlugokencky et al., 2005). Measurements made at a wide range of sites in both the Northern and Southern Hemispheres over the last 25 years show that the growth rate has decreased from greater than 1 percent $yr^{-1}$ (14 ppb $yr^{-1}$) in the later 1970s to early 1980s, to close to zero towards the end of the 1990s (Dlugokencky et al., 1998; Simpson et al., 2002). The reasons for the decrease and their implications for future changes in radiative forcing due to methane are not fully understood (IPCC, 2007). Some preliminary studies attributed the slow growth rate to decreasing anthropogenic emissions from fossil fuels, and it might be temporary (Bousquet et al., 2006; Evans, 2007). Simpson et al. (2002) pointed out, "the slowing of the $CH_4$ growth rate during late 1990s cannot be used to imply that $CH_4$ will no longer be of concern in greenhouse gas studies during this century." Andrews et al. (2004) shows data and a model that support the hypothesis that the leveling off is due to a reduction in emissions in the high northern latitudes from the former Soviet Union. Scientists do not believe atmospheric methane is at steady state and suggest the atmospheric burden of methane is likely to grow as third-world economies develop. In fact, according to a latest

study from GAGE/AGAGE (Global Atmospherics Gases Experiment/Advanced Global Atmospherics Gases Experiment) (Cunnold et al., 2002) and CSIRO (Australian Commonwealth Scientific and Industrial Research Organization) networks, global atmospheric methane mole fraction renewed its growth rate at the beginning of 2007 after almost a decade with little change in atmospheric methane concentration (Rigby et al., 2008).

The atmospheric $CH_4$ concentration results from a balance between $CH_4$ sources and sinks. A major portion of methane from natural sources is thought to originate from biological processes in anoxic conditions, e.g. from wetlands, rice paddies, etc. The major anthropogenic sources are ruminant animals and their waste, release from the mining and use of fossil fuels, anaerobic production from landfills, burning of biomass and rice paddy production (Evans, 2007). Emission from natural wetlands and rice paddies accounts for roughly half of the total $CH_4$ released to the atmosphere (Fung et al., 1991; Houweling et al., 1999). In addition, substantial quantities of methane clathrates have the potential to release large quantities of methane into the atmosphere producing a significant positive feedback on atmospheric temperature (Vourlitis et al., 1993). A recent study has made a remarkable claim that all terrestrial plants emit a substantial amount of methane into the atmosphere in the presence of oxygen (Keppler et al., 2006). This claim was not supported in subsequent reports (Dueck et al., 2007; Nisbet et al., 2009), and so the question remains open.

The major sink of atmospheric $CH_4$ is through photochemical destruction by the hydroxyl radical (OH) primarily in the troposphere (Bousquet et al., 2006), which accounts for more than 90 percent of the total loss (Lelieveld et al., 1998; Houweling et al., 1999). Methane oxidations in soil surface layers also play a role for the sink; although, it is not clear about the relative magnitude of methane loss due to oxidation in the soil as compared with photochemical destruction in the troposphere. More studies are needed to better understand factors that control methane exchange between soils and the atmosphere (von Fisher and Hedin, 2007).

The North American Carbon Program (NACP), and work done at the Global Monitoring Division of NOAA (GMD, formerly known as Climate Monitoring and Diagnostics Laboratory), have focused on processes affecting atmospheric $CH_4$ abundance and its impact on climate change. Two specific questions scientists are trying to answer are: (1) what are the sources, sinks and concentrations of $CH_4$, and (2) what are the factors that regulate these sources and sinks?

To answer these questions, methane concentrations and fluxes should be monitored on a global basis as we are now doing with $CO_2$. This will require a network of long-term and continuous flux and concentration measurements over various types of methane sources. Many of these sources include permafrost at high northern latitudes, Arctic tundra, dry land ecosystems, wetlands, rice paddies, and anthropogenic sources. Thus, a more complete record of long-term $CH_4$ flux from a wide range of sources and atmospheric $CH_4$ concentration measurements at representative locations is key to understanding source characteristics and how they might transform as the climate changes in the future.

Current closed-path methane flux measurements are restricted in time and space due to instrumental limitations. Until recently, instruments used for atmospheric $CH_4$ concentration measurements in the Global Atmospheric Watch (GAW) program of the World Meteorological Organization (WMO) and GAGE/AGAGE (Cunnold et al., 2002) were limited to gas chromatography or mass spectroscopy, which are not suitable for long-term and continuous field deployments. More recently, tunable diode laser-based instruments have become available; but so far, many of these closed-path instruments still have significant limitations.

For example, Billesbach et al. (1998) and Kim et al. (1998) used a tunable diode laser spectrometer with a closed-path configuration, which was developed by Campbell Scientific Inc., to measure flux over natural wetlands and rice paddies using eddy-covariance techniques. This instrument uses a liquid nitrogen cooled lead-salt tunable diode laser. To avoid the problems associated with using liquid nitrogen, Aerodyne Inc. (http://www.aerodyne.com) developed a $CH_4$ analyzer using a closed-path, multi-pass Herriott optical cell and a thermo-electrically cooled quantum cascade laser operating at various wavelengths, which has a resolution and response time suitable for eddy-covariance measurements (McManus et al., 2002; Nelson et al., 2004; Kroon et al., 2007). However, this instrument weighs over 160 lbs and requires 300 W of power. Los Gatos Inc. (http://www.lgrinc.com) has also developed a closed-path, fast response $CH_4$ sensor, using a technique related to cavity-ring down spectroscopy called Integrated Cavity Output Spectroscopy (ICOS). The ICOS technique requires the use of relatively large diameter mirrors with each having a very high reflectivity (R~0.9999). Thus, their optical paths have large cell volumes (0.55 liter) and must be extremely clean. These instruments are also large and require mains power (~825 W). Two $CH_4$ instruments (Model G2301, G2311) introduced by Picarro Inc. (http://www.picarro.com) use cavity ring-down spectroscopy and have cells with smaller volume (about 35 $cm^3$) but still require extremely high mirror reflectivity and mains power (~470 W). Picarro $CH_4$ analyzers appear not to support the fast response sampling (10Hz) as required for eddy-covariance flux measurement.

Large cell volume, closed-path analyzers are not ideal for fast response eddy-covariance flux measurement, simply because flow rates on the order of several hundred liters per min are required (e.g. McManus et al., 2002; Nelson et al., 2004; Hendriks et al., 2008). For example, if a measurement requires a 10 Hz bandwidth, then the instrument response would have to be twice that rate, or 20 Hz, which is 20 air changes per second. If the instrument has a cell volume of 0.5 L, then 20 air changes per second requires a flow rate of 10 liters per second; that's 600 LPM (liters per min) at the operating pressure of the cell. If the cell operates at 0.05 atm, then the incoming flow rate at one atmosphere would have to be 0.05 x 600 = 30 LPM. If a 5 Hz bandwidth is adequate, then a flow rate of 300 LPM at the cell operating pressure would be required, which is equivalent to 15 LPM at one atmosphere. These high flow rates are necessary to flush out the sample cell rapidly enough to support the fast response required by the eddy covariance method. Further complicating the problem, these high flow rates must be maintained against substantial pump head pressure because the instruments operate at reduced optical cell pressure, which produces high resistance to flow. Thus, the pumps require about 500 W of power to maintain adequate flow rate. For example, for a 10 Hz sampling rate, a 0.5 L cell changed 10

times per second and operated at 0.05 atmospheric pressure requires (1-0.05)x$10^5$ J $m^{-1}$ x 10 x 0.5x$10^{-3}$ $m^3$ $s^{-1}$ = 475 W of power. This assumes perfect efficiency and does not include additional power to operate the instrument.

The large cell volumes, high power consumption and cryogenic lasers used in existing closed-path methane analyzers present practical limitations and problems when considering requirements for long-term flux and atmospheric methane concentration measurements in remote areas. Mains power is often not available, and requirements for liquid nitrogen make unattended and remote operation difficult. The combination of high flow rates and the requirement for extremely high mirror cleanliness may make cleaning intervals frequent. For these reasons, currently available closed-path methane analyzers are not ideal for eddy covariance measurements or for other applications at remote field sites on a long-term basis. The Los Gatos, Picarro and Campbell Scientific instruments have been successfully deployed for eddy covariance applications, but such deployments require mains power and sometimes labor intensive efforts. Generators could be used for remote deployments but could negatively influence the $CO_2$ and $CH_4$ measurements (Detto et al., 2011).

We believe a valuable alternative for making eddy covariance flux measurements, to these closed path instruments, is an open-path $CH_4$ analyzer. We currently sell an open-path methane analyzer, the LI-7700, which was developed under DOE SBIR Project (DE-FG02-05ER84283). Our open-path methane analyzer began production in the spring of 2010. Since beginning to sell this instrument, it has demonstrated a typical sensitivity (RMS noise) of 5 ppb at 10 Hz at 2 ppm. The instrument has a 50 cm mechanical path length, weighs less than 4 kg, and has a system to actively and automatically clean the lower mirror. The 7700's ability to clean and heat the mirrors minimizes the loss of data for moist conditions, and the design provides continuous, long-term measurements over the desired fetch without disrupting the natural environment. (Dengel et al., 2011). The instrument operates at a nominal power of 8 W and can be operated using solar power. According to Detto et al (2011) the open path analyzer is suited for remote sites and data loss due to instrument failure was nine percent less than compared to the Los Gatos Research closed-path fast methane sensor. McDermitt et al (2010) reports that co-spectra collected from the LI-7700 is comparable to the theoretic curve in the surface layer.

The current design of our $CH_4$ analyzer, which is being developed under this DOE SBIR Phase II Project (DE-FG02-05ER84283), will provide the scientific community with a field deployable, closed-path option. The first generation prototype of the closed-path $CH_4$, $CO_2$, and $H_2O$ analyzer instrument (α-version) is currently being assembled with the optical bench being tested. The expectation is that the analyzer will weigh < 9 kg, consume < 12 W of power (analyzer only); and will perform with a sensitivity (RMS Noise) on the order of 6 ppb at 10 Hz at 2 ppm. Furthermore, optics will be accessible and cleanable by the scientist on site.

LI-COR is recognized as a world leader in designing and manufacturing gas analyzers for scientific research. We have been designing and manufacturing accurate and robust gas analyzers for more than 20 years. Our closed-path and open-path $CO_2$, $CO_2$/$H_2O$, and $CH_4$ gas analyzers include the LI-6252, LI-

6262, LI-7000, LI-7200, LI-7500A, LI-7700, LI-800, LI-820, and LI-840. These instruments have made important contributions to ecosystem carbon budget research. The LI-6262, LI-7000, LI-7500, and LI-7700 were revolutionary advances in environmental instrumentation. According to the Fluxnet website (http://www.fluxnet.ornl.gov/fluxnet/siteinstrumentindex2.cfm), more than 95% of carbon flux research sites are using LI-COR gas analyzers. Many observation sites in the GAW program of the WMO also use LI-COR closed-path $CO_2$/$H_2O$ analyzers, including the LI-6252, LI-6262 and LI-7000, to continuously monitor atmospheric $CO_2$ concentration on a long-term basis. Our instruments are deployed in a wide range of environmental conditions, from Arctic tundra to tropical mangroves, and have been widely used in environmental science, climate change research, ecology, plant biology and agricultural science.

We expect our current open-path methane analyzer and the in-design closed-path methane, carbon dioxide, and water vapor analyzer (supported by a current DOE SBIR Phase I and Phase II grant) will support the large scale deployments that will be necessary to achieve a better understanding of the global $CH_4$ and $CO_2$ budgets. Further, we believe that such analyzers designed to be environmentally robust and operate without the need of mains power will make a large impact on global climate change research, as have our current $CO_2$ gas analyzers.

## 2.1 Instrument Description

The closed path analyzer will be an excellent instrument to measure $CH_4$, $CO_2$, and $H_2O$ flux over various ecosystems. It requires only about 30 W of power during normal operation, which means that the entire system can be operated with solar panels in a remote location. The analyzer will be able to communicate to a data logger or computer via Ethernet or RS-232, connect to various sonic anemometers via RS-232, RS-485, or analog, and connect to secondary sensors via 8 analog I/O channels.

## 2.2 Instrument Preliminary Specifications

| | |
|---|---|
| Operating Temperature: | -25° to 50°C |
| Power Requirements: | 10.5 – 30 VDC |
| Power Consumption: | < 12W (analyzer only), < 30W (with pump) |
| Resolution $CH_4$: | 6 ppb at 10 Hz |
| Calibration Range $CH_4$: | 0 – 71 μmol/mol (ppm) |
| Resolution $CO_2$: | 0.075 ppm at 10 Hz |
| Calibration Range $CO_2$: | 0 – 2600 μmol/mol |
| Resolution $H_2O$: | 0.0036 mmol/mol at 10 Hz |
| Calibration Range $H_2O$: | 0 – 60 mmol/mol |
| Communication: | Ethernet or RS-232 |
| Sample Rate: | 40 Hz |
| Physical Bandwidth: | 10 Hz |
| Input/Output: | Ethernet, RS-232 x 2, RS-485, Analog I/O x 8, Power |
| Application Software: | OS X, Linux, Windows OS, Embedded Web Server |
| Weight: | < 9.0 kg |

# 3.0 Theory

## 3.1 Wavelength Modulation Spectroscopy (WMS)

Gas molecules absorb photons at specific wavelengths; this process is described by the Beer-Lambert law. Tunable diode laser spectroscopy (TDLS) utilizes the narrow emission from diode lasers for probing specific absorption lines of molecules of interest. Diode lasers in the telecommunication range are commonly used for TDLS measurements but can be restricted to overtones of primary absorption features. These overtones have much lower absorption than the primary bands and produce very low signals when trying to make direct measurements of the absorption features.

WMS uses a diode laser to probe a gas sample much like a direct detection technique but modulates the wavelength of the laser across the absorption feature for improved detection of the residual. The emission spectrum of the laser is simultaneously scanned with a ramp across the absorption line and a high frequency sinusoid at a modulation frequency f. The resulting spectral scan is demodulated using a synchronous harmonic to recover a representation of the absorption line.

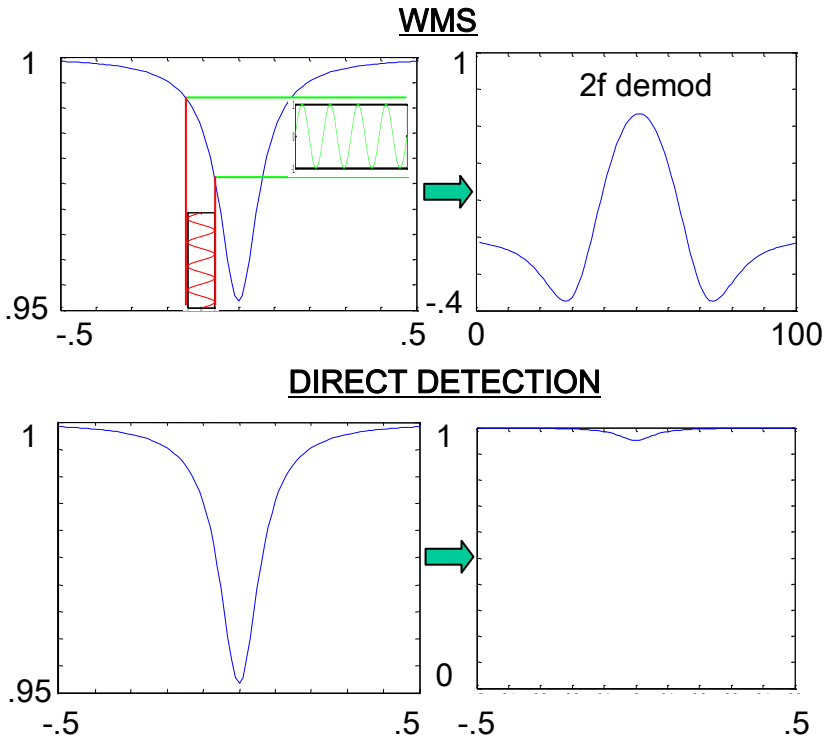


Figure 1: Comparison of WMS and Direct Detection Theories

Demodulation frequencies are at $nf$, where the resulting signal is proportional to the nth derivative of the line shape. As the modulation depth, or amplitude of the sinusoid, approaches zero, the signal

approaches the derivative of the absorption line shape. However, optimal signal is achieved when the modulation depth is at 2.2X the line width of the absorption line. Greater detection sensitivities can be achieved, but at the expense of losing spectral information about the line shape.

## 3.2 Direct Absorption

In the 2002-2003 nm region at atmospheric pressure, the spectra of water and $CO_2$ significantly overlap as demonstrated in Figure 2. The cross talk between two spectra can be separated and provide a baseline when working at low pressures of 50-100 Torr. At low pressure, however, a vacuum pump capable of high flow rates providing at least a 10Hz response would be necessary and would increase the power consumption beyond our desired value. Instead, we use a reference signal either from another photodiode placed before the absorption cell or a prerecorded signal in the absence of any absorber during the calibration with the zero gas.

From the Beer-Lambert Law, the received optical power is proportional to the incident power before entering the absorption cell $I = I_0 e^{-\alpha}$. The signal from the baseline channel is proportional to $I_0$. Then $I_{sig} = R I_{base} e^{-\alpha}$ where $R$ is the ratio of power levels on two photodiodes. Taking the natural logarithm of it becomes $ln(I_{sig}) = ln(R) + ln(I_{base}) - \alpha$. Since $ln(I_{base})$ is known, it can be subtracted. The $ln(R)$ is for a single sweep at a constant value. The problem with fitting the $ln(I_{sig})$ to the absorbance becomes a linear one which can be solved by linear regression using Singular Value Decomposition (SVD). When relative power levels change due to contamination or other factors, the change in $ln(R)$ only affects the offset.

Individual spectra for $CO_2$ and water are pre-calculated from the high-resolution transmission molecular absorption database (HITRAN) with high accuracy for a range of temperature and pressure values and a predetermined scan range. The results from SVD fit vectors are stored in the instrument memory and then the actual fit vectors are determined from that table by bilinear interpolation. The grid is sufficient to provide high accuracy for the fit vectors in a full operating range of 50-110 kPa and -25˚ to 50˚ C.

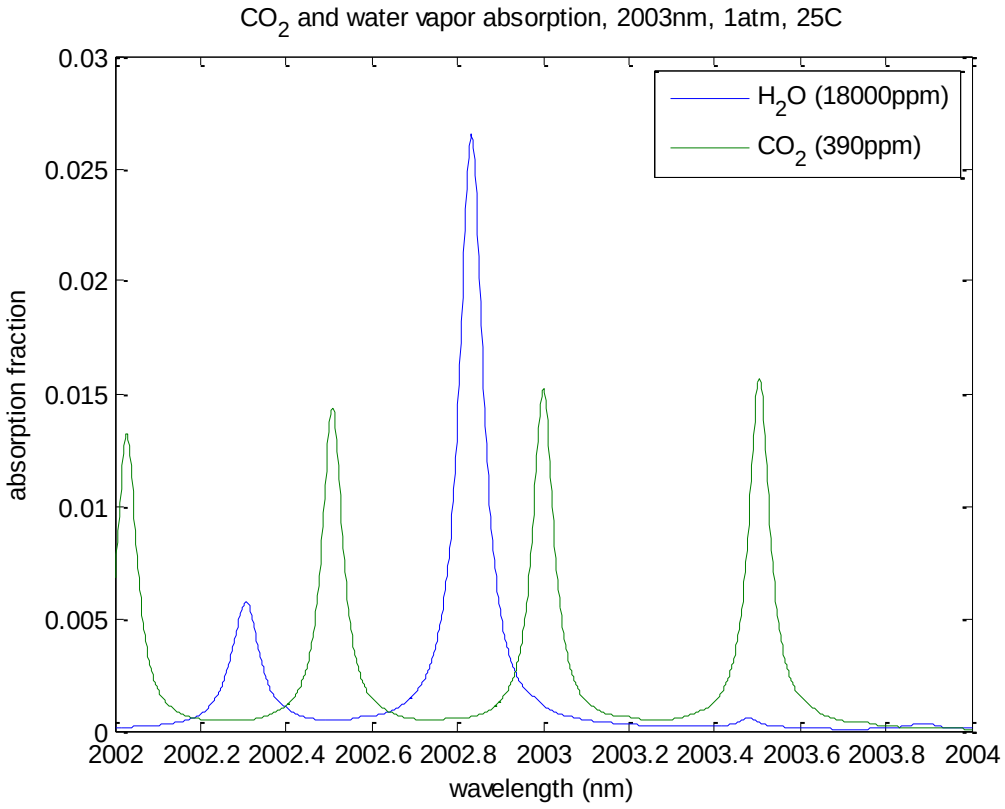


**Figure 2: $CO_2$ and $H_2O$ Absorption Lines at 2003 nm**

Compared to Distributed Feedback Lasers (DFB), Vertical-cavity Surface-emitting Lasers (VCSELs) have a relatively wide scanning range, so few lines can be scanned in a single sweep. If two or more $CO_2$ lines are scanned, their peak positions in the reference gas cell can provide direct information about the wavelength tuning curve of the laser. In the case of three or more lines, the non-linearity of the laser tuning ramp can be determined, and then the ramp can be adjusted to linearize the scan to lock laser temperature, bias and sweep range.

Since temperature (T) and pressure (P) are known and fit vectors are specifically calculated with high accuracy for a given temperature and pressure, the fit is more accurate than a single line and less susceptible to small residual fringes. This method also provides a high dynamic range because the absorbance is linearly proportional to the concentration, and there is no saturation to the analog to digital (A/D) converter. Only the absolute resolution would decrease with increasing concentration while maintaining relative resolution.

Given that both the water and $CO_2$ spectra are independent to the first order, there is no crosstalk between them. It is still possible that there could be a small interdependence mostly due to potentially non-negligible water vapor broadening of the $CO_2$ lines which we intend to study in more detail once the alpha-prototypes are complete.

## 3.3 Optical

The dominant noise source for either WMS or direct absorption measurements are Fabry-Perot etalons. When making either absorption measurement, the signal that results from an absorption profile causes a change in intensity of the light that is a function of the wavelength emitted. Low finesse fringes are caused by optical interfaces or stray reflections from surfaces, which causes spurious optical paths within the system and result in constructive and destructive interference. This interference causes sinusoidal changes in intensity of the light that is a function of wavelength and is indistinguishable from frequency components of the absorption feature.

Absorption features such as $CH_4$ at 1651 nm will cause a change in intensity of about 1 part in $10^3$. Resolution of the changes in amplitude of this absorption feature needs to be around 1 part in $10^6$. Conventional antireflective coatings can be designed for about 1 part in $10^3$ back reflections. Typically with careful design, 1 part in $10^5$ to $10^6$ is achievable for an entire system. Numerous methods are used for obtaining low back reflection values and no single method is completely effective.

Techniques for obtaining low back reflection:

1. Using antireflective coatings to attenuate optical power of stray reflections.
2. Chose thicknesses of optical components such that the frequencies of any fringes present are not similar to any frequencies contained in the line shape. These fringes will then be filtered out in any curve fitting algorithms.
3. Roughen surfaces that are causing stray specular reflections. This diminishes the power present in the parasitic paths.
4. Blacken surfaces. This is not always effective since many black paints are reflective in mid infrared.
5. Actively dither elements that cause fringes. This randomizes the phase of the etalons and converts a low frequency slow drifting noise to a higher frequency that can be averaged.
6. Spread spectral reflections as far apart as possible to avoid small amounts of scattered light at interfaces.

## 3.4 Digital vs. Analog Signal Conditioning

Digital signal conditioning is a method of processing where the photodetector signal is sampled with a high speed analog to digital converter as early as possible in the receive signal processing chain. This design provides both advantages as demonstrated by the lab prototype and disadvantages that have already been addressed during the design phase.

Digital signal conditioning offers several appealing advantages. First, it reduces offset error in the WMS demodulator caused by non-ideal behavior of the equivalent analog circuit. It also provides a straightforward and offset free method of performing logarithmic pre-processing on both WMS and direct absorption signal chains. Digital conditioning offers generally lower power consumption for the overall assembly, and smaller overall physical size and cost of the components necessary to implement the design. Finally, there is an element of flexibility, allowing relatively easy transitions from WMS processing to direct absorption processing as new information is collected on the best practice for each gas species.

There are also a few disadvantages of the digital signal conditioning method. First, the design is more complex, and therefore, requires the use of more highly integrated digital logic and digital signal processing integrated circuits. In addition, the higher sampling rates tend to complicate the selection of appropriate analog to digital converters and the associated amplifier circuitry that drives them. Finally, the method demands relatively high data throughput rates at points in the design, dictating larger and more powerful processing elements.

# 4.0 Instrument Design

## 4.1 Optical and Mechanical Design

### 4.11 Reference Cell Design-Dual Laser

Two lasers, one operating at 1651 nm and the other at 2003 nm, are combined into a single beam using a dichroic prism. This prism has coatings for combining the light into two separate beams that each contains light from the lasers. The majority of the light is directed to a sample cavity which contains the analytes and the rest directed to a wavelength reference assembly.

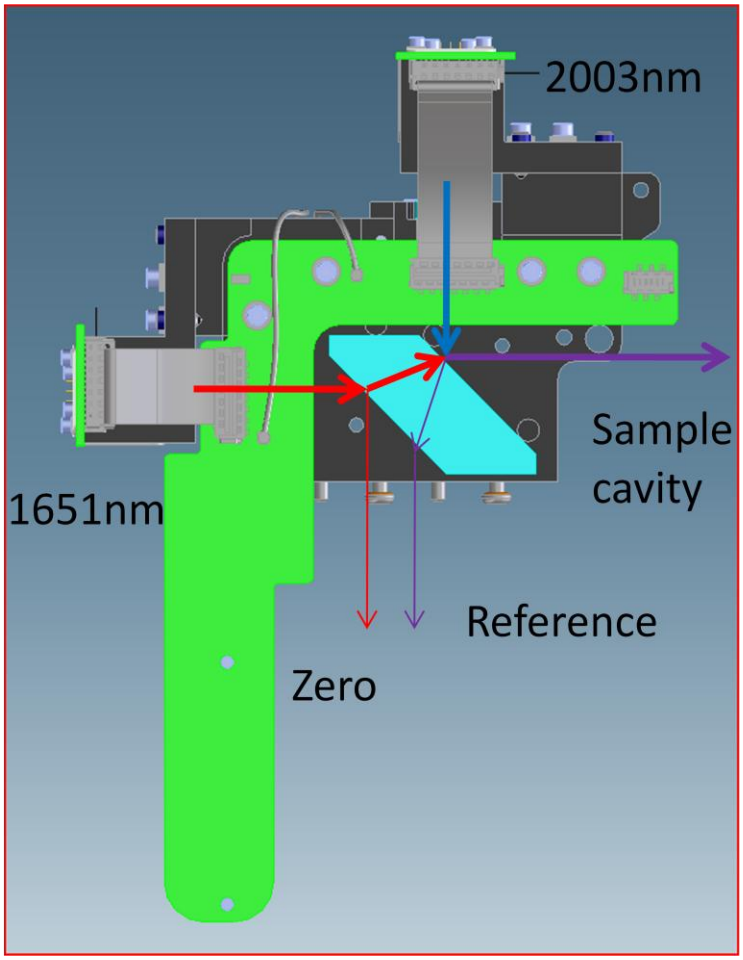


**Figure 3: Most of the laser power exits to the right. A small percentage is directed to a wavelength reference assembly. These are depicted as Reference and Zero in the figure.**

The dichroic element is designed to reflect approximately 5 percent of the 1651 nm beam from the first surface to a photodiode, which we call a zero reference path. Another 5 percent is reflected from the second surface and directed to a wavelength reference path, which contains a small volume of $CH_4$. The 2003 nm beam impinges on the second surface of the dichroic where 95 percent of the light is reflected to the sample path. Approximately 5 percent is transmitted through the dichroic to the wavelength reference path. An "L" shaped circuit board attaches to this assembly and contains laser driver circuitry and photodiode amplifiers.

Utilizing this same dichroic on the return path allows the light to be split back into individual wavelength components and imaged onto separate photodiodes. This reduces the number of optical elements in the system and allows for a high degree of separation between the two optical channels. This enables a move away from time division multiplexing (TDM) and allows the performance of simultaneous measurements. The expected power in each of the channels based on individual components is given in the table below.

| | T (percent) | T (db) |
|---|---|---|
| Detector 1, 1651 nm | 68 | -1.7 |
| Detector 1, 2003 nm | .00000175 | -67.6 |
| Detector 2, 1651 nm | .000149 | -48.3 |
| Detector 2, 2003 nm | 72.2 | -1.4 |

Table 1: Comparison of Detectors

### 4.12 Sample Volume Design

The sample cell was designed to characterize the sample volume of gas, to easily perform maintenance of the cell, and to minimize the change in distance between the mirrors over the temperature range of the instrument.

The average sample cell temperature is characterized by measuring the inlet and outlet sample gas using fine wire thermocouples. These thermocouples have a suitable frequency response in measuring fast fluctuations in the temperature of the incoming sample cell gas.

To characterize the pressure within the sample cell, an absolute pressure transducer was implemented in the center of the sample cell to find an accurate average sample that will account for the head loss within the cell.

The sample cell was configured to allow easy maintenance, part replacement and cleaning. The thermocouples, made of delicate wire, may need to be occasionally replaced and can be accomplished by removing the inlet and outlet sections. The bottom mirror and interior sections can also be removed to allow the user to clean the cell walls and mirrors. Machined pads are used to provide consistency so that the user can repeatedly remove the mirrors and reposition them in the correct setting. This ensures that the critical path length remains unchanged.

It was also imperative to keep the distance between the sample cell mirrors constant over the temperature range of the instrument, and this was accomplished by using Invar (64FeNi) for the tube design. This Nickel-Steel alloy has a low coefficient of thermal expansion; therefore, the change in length of the sample cell and distance between the mirrors is insignificant over the operating temperature range.

### 4.13 Detection Methods-Wavelength Reference

Two beams of light enter the reference assembly, one for wavelength reference and another for a $CH_4$ zero measurement. The reference beam for monitoring and controlling the wavelength of the laser modules contains light from each laser module. This light is passed through a small, enclosed volume containing $CH_4$ and $CO_2$. Combining the wavelength reference gases into a single volume minimizes the cost and complexity of the assembly. Only a single hermetically sealed volume is required and fewer optical elements are needed for directing the beams into separate channels.

After the beam is transmitted through the reference sample cell, a spherical mirror focuses the light through another dichroic element and then onto two photodiodes. Partial pressures of $CO_2$ and $CH_4$ were chosen such that $CO_2$ would not be visible in the $CH_4$ channel and vice versa.

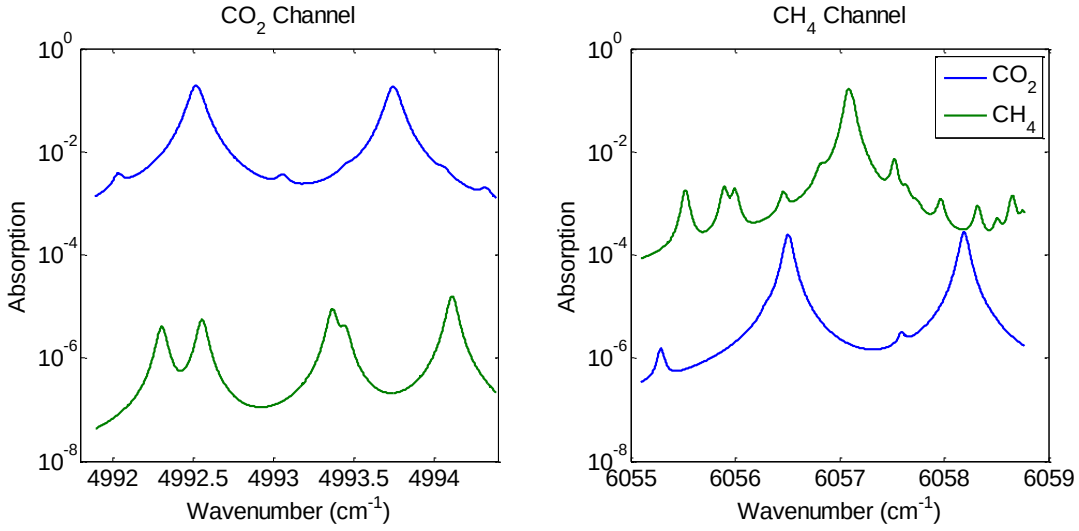


**Figure 4: A partial pressure of 80 Torr $CH_4$ and 320 Torr of $CO_2$ are used in a single enclosed volume for a reference absorption measurement.**

A reflection from the front face of the dichroic is also used to monitor laser power of the 1651 nm laser. This signal provides a baseline scan of power fluctuations of the laser and can be used for normalizing the signal from the laser cavity. Noise sources from the laser, such as Fresnel reflections from the collimating lens, could potentially be removed from the signal more effectively than dithering techniques. Dithering techniques involve moving an optical element causing multiple beam interference rapidly compared to data acquisition rates. The phase of the sinusoidal noise caused by the interference is then randomized and the noise source, over time, will average to zero.

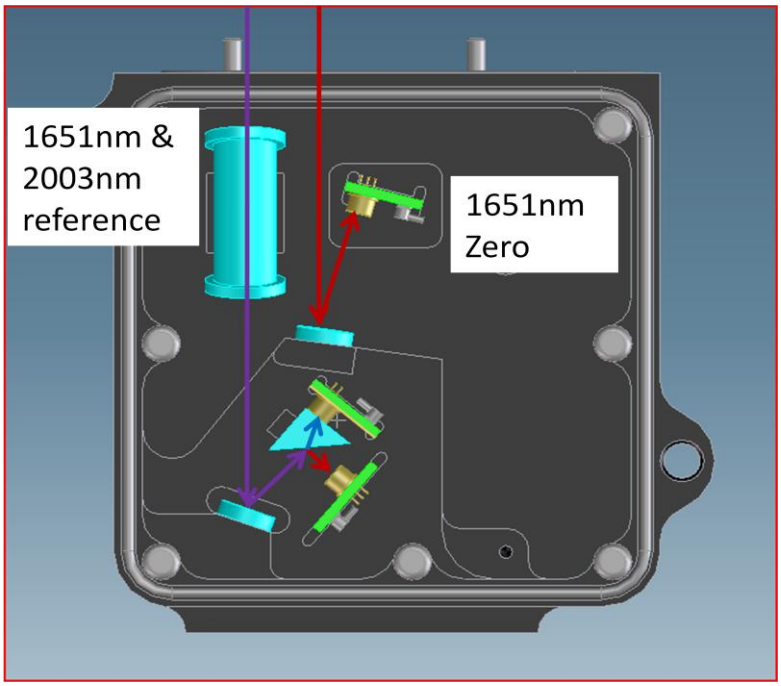


Figure 5: Reference and Detector Placement

## 4.2 Electrical Design

### 4.21 Architecture

The electronics design architecture for the closed-path analyzer is similar in design to our previously developed open path trace gas analyzer but has been modified to include the measure of $CO_2$ and $H_2O$. To effectively measure all three gases, the closed-path analyzer uses two optical paths and laser packages.

The electronics control the excitation light sources, process the received signal, and analyze the signal to recover a gas concentration. As discussed later in this report, the electronics also provide a user interface for control and presentation of data. The signal chain begins with excitation control. The control circuit is a low noise injection current source which provides a DC injection, modulation and sweep current. To regulate the mean wavelength of the VCSEL lasers, a thermoelectric cooler is provided with each laser and its cooling capacity is regulated by a temperature control circuit using a thermistor temperature sensor integrated in the laser package. The optical responses from the reference and sample cells are sensed by a pair of PIN photodiodes and then demodulated to produce the WMS response signal. The WMS signals are sampled by a digital signal processor (DSP) and analyzed to produce a concentration signal. The results are then communicated to the user via a DAC driven analog output or wired Ethernet connection.

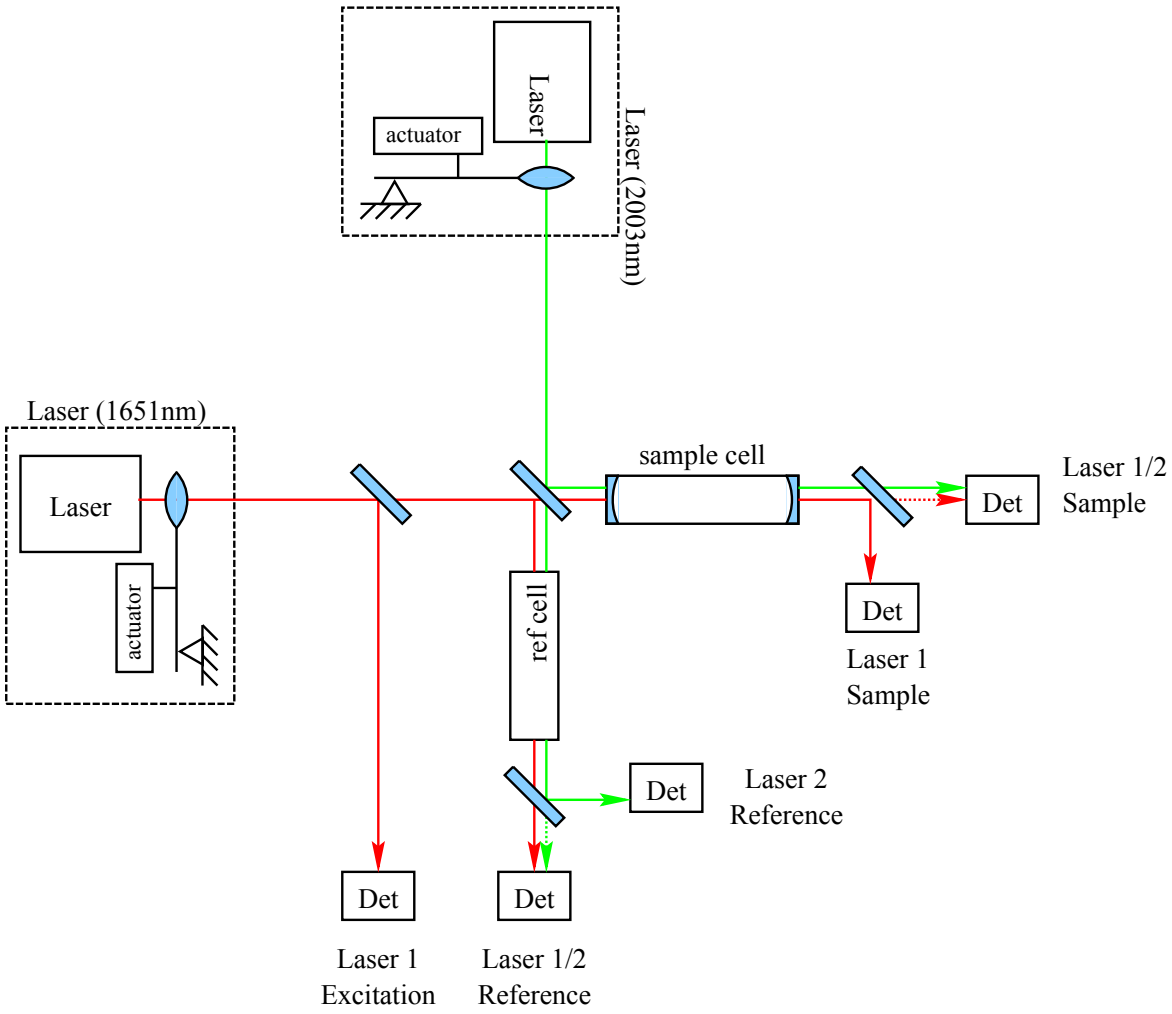


Figure 6: Optics Block Diagram

As indicated in Figure 6 of the block diagram schematic, the design contains two lasers each having associated optics and reference cells coupled in to the sample volume. The sample and reference cell outputs each contain diachroic optics to separate the two laser colors onto individual detectors. The 1651 nm laser has a separate photodetector channel to sense etalons in the laser package and normalize the measurement. The photodetector channel provides point-by-point removal of major drift normally occurring from etalons in the laser assembly. This allows an independent measure of the optical power of each laser to promote laser signal separation.

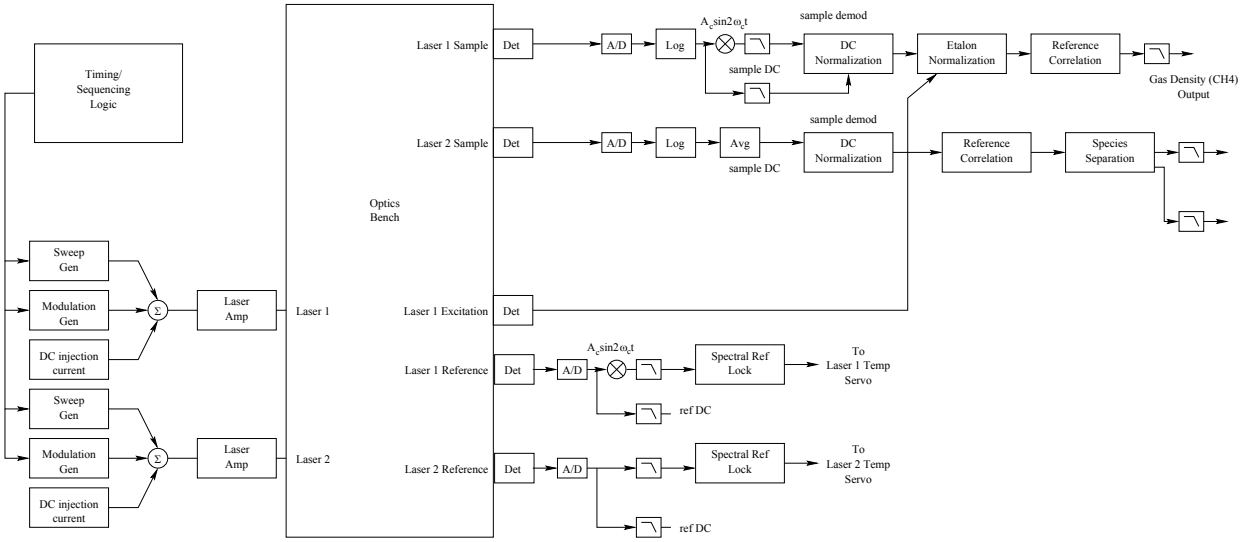


**Figure 7: Electronics Block Diagram**

## 4.22 Digital Design

The digital design for the $CO_2/H_2O$ channel uses a direct absorption technique. The $CH_4$ channel uses digital demodulation. Because this uses a high speed digital process which requires extra processing, a larger FPGA device was implemented.

## 4.23 Analog Design

Two filtering methods are used in the closed-path analyzer. First, an analog pre-filter is applied to the detector signal to limit the detector bandwidth to prevent aliasing. This filter allows energy associated with valid line shapes to pass while eliminating noise and etalons that exist outside the line shape bandwidth. The filter also rejects demodulation products and conditions the signal for sampling by a high speed A/D converter. After the demodulated signal has been fitted and converted to a concentration, a second moving average post filter may be used to further limit system bandwidth as required.

## 4.24 Challenges

There have been a number of challenges to the hardware design for this instrument. The first challenge was in developing a processing method that could both improve on the LI-7700 electronic design, and accommodate the new requirements of the second laser channel. In addition, the feature set required by the new instrument, coupled with the power requirements needed for the instrument to be competitive, required a careful examination of power consumption in all aspects of the design.

# 4.3 Software Design

The instrument software can be separated into three primary categories:

1. Application: Client Software Package
2. Communication Protocol
3. Embedded Software Package & Web Server

### 4.31 Application: Client Software Package

The client software package represents the user interface and will provide the user with a simple and comprehensive mechanism which can be used to configure all aspects of the instrument operation. The embedded software package is the software onboard the instrument itself and is used to govern all aspects of the instrument's performance from the moment the instrument is powered up. While the development of the embedded software package is centered on a combination of the instrument performance specifications as well as the actual hardware used, the client software package can be much more flexible in the way that it presents data and control parameters to the end-user. As such, it will be revised after intensive reviews by LI-COR and external scientists. The communication protocol will link the application with the embedded software.

The client software package will be a stand-alone software package currently targeted to the following user PC platforms:

- Windows (XP, Vista, 7)
- Linux (Ubuntu, Fedora)
- Apple (Mac OSX or higher)

It shall be used to configure the instrument using one of the standard PC platforms listed above through a dedicated RS-232 connection, or a network TCP/IP connection. The connection is made by pressing the "connect" toolbar button ($4^{th}$ button from the left which has the appearance of a cable with a connecting socket on the end, see Figure 10.) Doing so will open the connect dialog as shown:

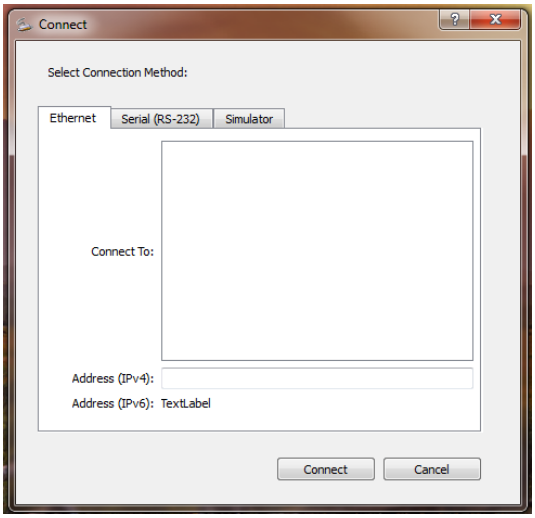


Figure 8: Connect Dialog with Ethernet Selected

The dialog has three separate tabs indicating two possible connection methods (Ethernet and RS-232) as well as an onboard simulator that the user may choose to run without needing to connect to an actual instrument, which can also be utilized for teaching and learning how to operate the analyzer. If the Ethernet connection is selected, the user will be presented with a list box holding the name of the instrument. In the event that the instrument name does not appear in the list box, the user may enter the instrument Internet Protocol (IP) address manually. If the user wishes to connect via RS-232, the user simply selects the RS-232 radio button and then picks the desired communication channel as shown Figure 9.

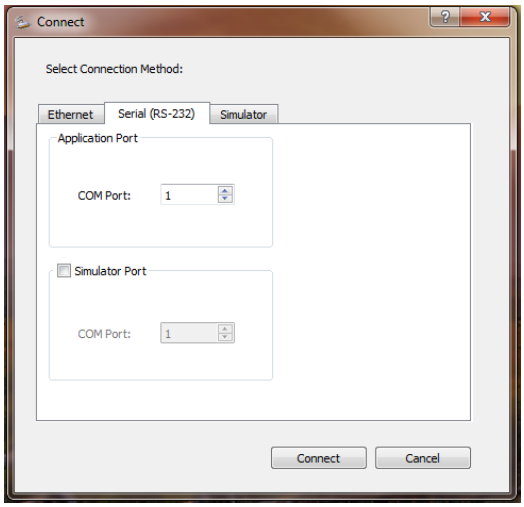


**Figure 9: Connect Dialog with RS-232 Selected**

When the client application connects to the instrument, the following screen will be updated with actual data values as shown:

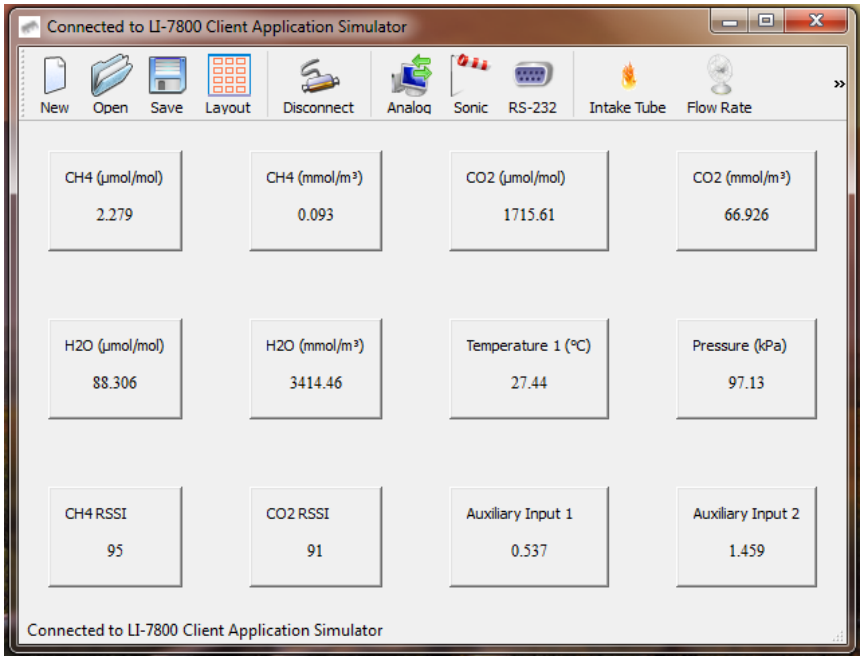


**Figure 10: Main Application Screen of Client Application Software Package**

The primary display will contain the data values currently generated by the instrument (e.g., $CH_4$, $CO_2$, $H_2O$, temperature, pressure, and possibly eight auxiliary input channels). The "possibly" qualifier is placed on the input channels for the basic reason that they will be "bi-directional" channels which may be configured as auxiliary inputs, or as Digital Analog Converter (DAC) outputs. The I/O configuration will be set by the user, as illustrated later. Once a connection is made, the data values will display in numerical format. Should the user wish to view the data graphically, the user would simply press the graphing button located in the lower left corner of each numerical data display panel. This will cause a chart to appear which can be independently scaled and positioned as shown in Figure 11.

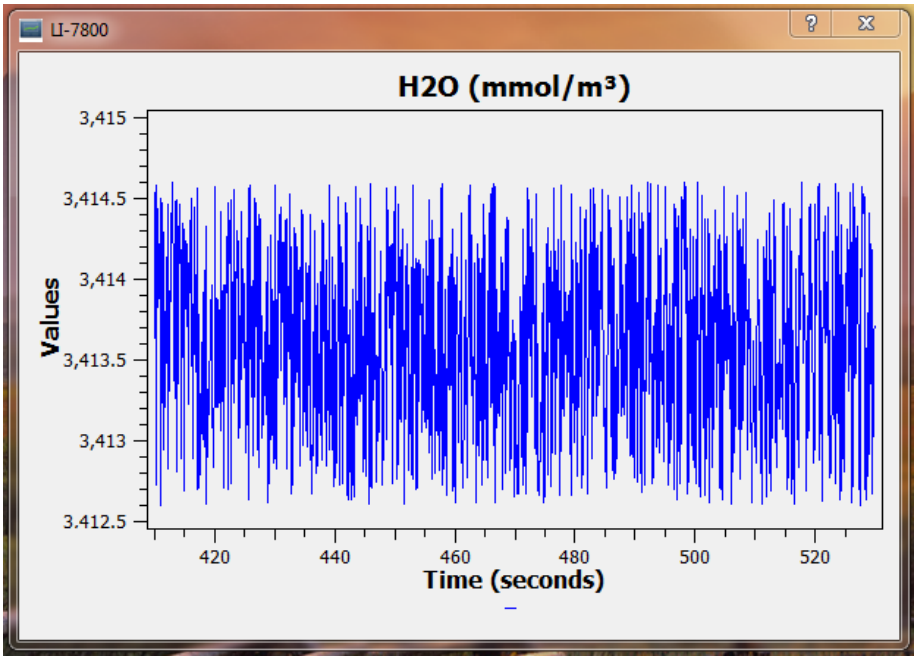


Figure 11: Real-time Chart showing an example of a simulated time series of water vapor density (mmol $m^{-3}$)

### *4.311 Instrument Configuration*

The instrument shall store, and internally maintain, a configuration for operation even when powered down. This configuration will be passed to the client application when the initial connection is made. Optionally, a new configuration can be loaded into the client application and then passed from the client to the instrument when the connection is made. To load the configuration from a file on the client PC, the user would simply press the folder icon on the toolbar. (2nd from the left, see Figure 10) This will open the following dialog. See Figure 12.

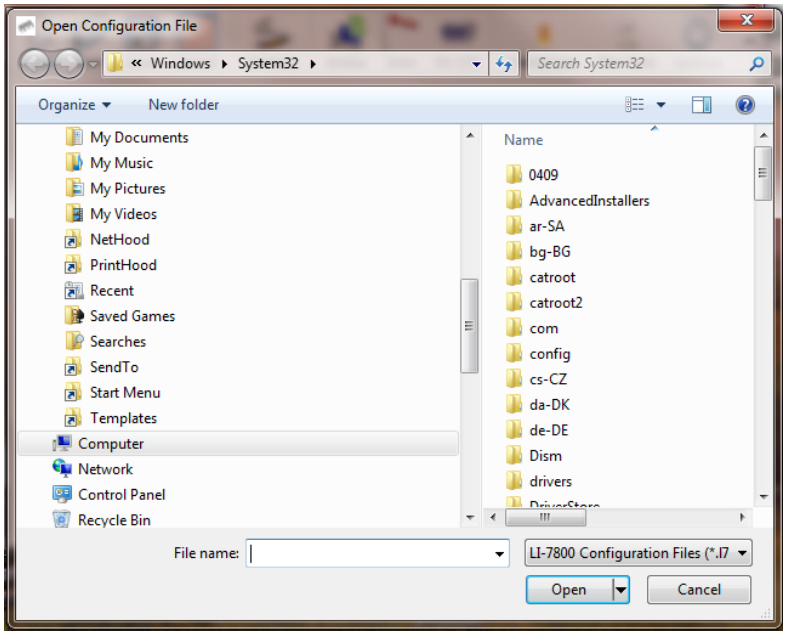

Figure 12: Load Instrument Configuration from File

Loading the configuration file can be done while the application is not connected to the instrument. This allows the user to pre-define the instrument configuration prior to connecting to it. It will also be possible to save an instrument configuration (whether retrieved from the instrument itself or defined in a disconnected mode by the user) by pressing the floppy disk icon on the toolbar (3rd icon from the left, see Figure 10). This will open the save configuration dialog as shown in Figure 13.

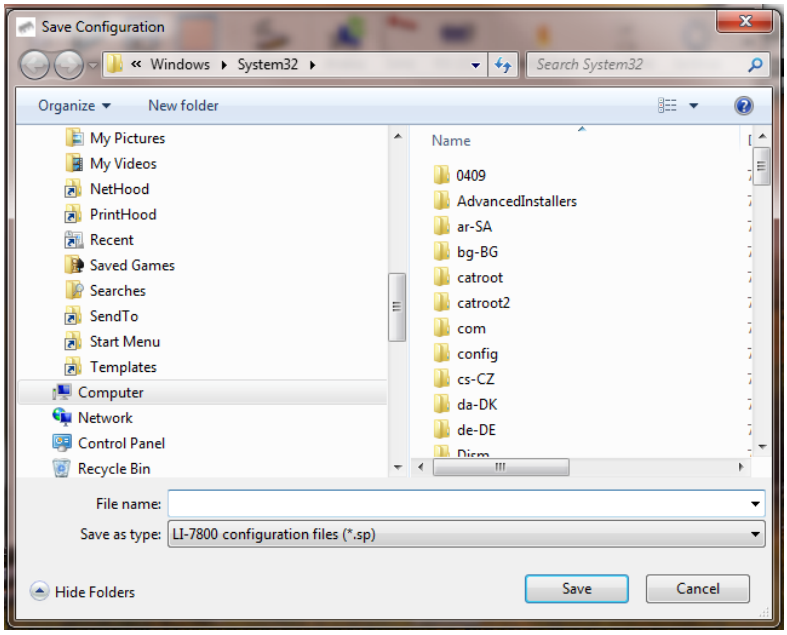


Figure 13: Save Configuration Dialog

### *4.312 Bi-directional Analog Channels*

As stated previously, the instrument will have eight "bi-directional" analog channels. These channels may be configured as analog input channels or as DAC output channels. For either option, the user would select the analog configuration button on the button bar (5th button from the left, see Figure 10) to bring up the analog channel configuration dialog as shown in Figure 14.

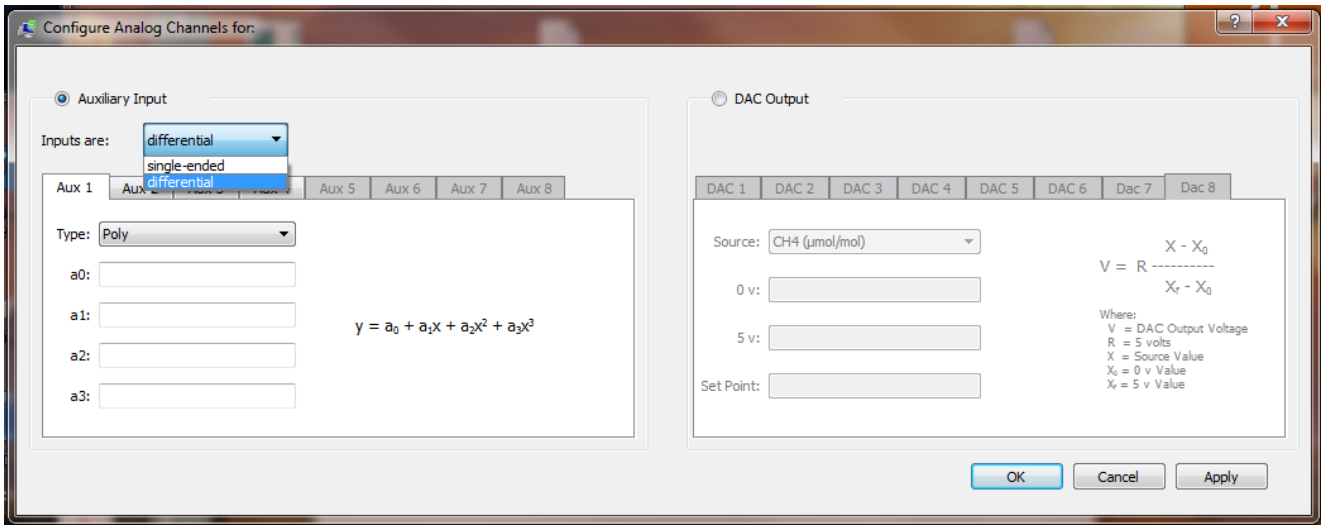


**Figure 14: Analog Channels Configured for Analog Inputs**

The analog channels may be configured for input or output, but not both simultaneously. Figure 14 indicates that the channels are configured for analog inputs. As such, there are two possible configuration options (generic polynomial or thermistor).

If set for the generic polynomial input, the channels will employ a polynomial equation of the form:

$$Y = a_0 + a_1 x + a_2 x^2 + a_3 x^3$$

in order to determine the input signal value.

If set for thermistor input, the channels will employ a Steinhart-hart equation of the form:

$$R_t = \frac{a_0 V_{aux}}{5V - V_{aux}}$$

$$T = \frac{1}{a_1 + a_2 \ln(R_t) + a_3 \ln(R_t)^3} - 273.15$$

in order to determine the input temperature value.

Should the user wish to use the analog channels as output channels, the user would simply select the DAC Output radio button. This will alter the dialog as shown in Figure 15.

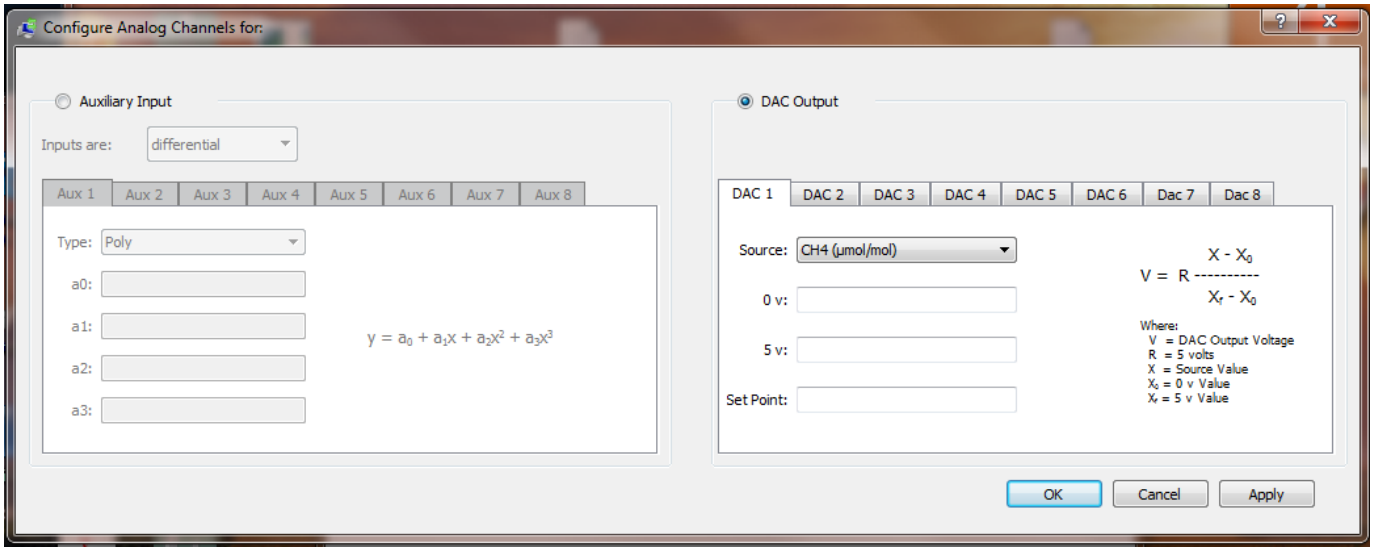


**Figure 15: Analog Channels Configured for DAC Output**

When used in this configuration the channels shall provide a voltage output scaled from 0V – 5V by the user settable parameters following the corresponding equation:

$$V = R\frac{X - X_0}{X_f - X_0}$$

where:

$V$ = DAC Output Voltage
$R = 5\ volts$
$X$ = Source Value
$X_0 = 0v$ Value (e.g. 0 volts corresponds 0 ppm $CO_2$)
$X_f = 5v$ Value (e.g. 5 volts corresponds 1000 ppm $CO_2$)

The source shall be one of the following primary variables displayed on the main form (e.g., $CH_4$, $CO_2$, $H_2O$, temperature, pressure, etc.).

### *4.313 Flow Control*

The instrument will be designed to interface with an external flow control unit. This interface shall be accomplished with an RS-485 connection. In this configuration, the user will be able to set the flow control by pressing the Flow Control tool bar button ( $10^{th}$ button from the left with a fan image, see Figure 10). This will bring up the flow control dialog as shown in Figure 16.

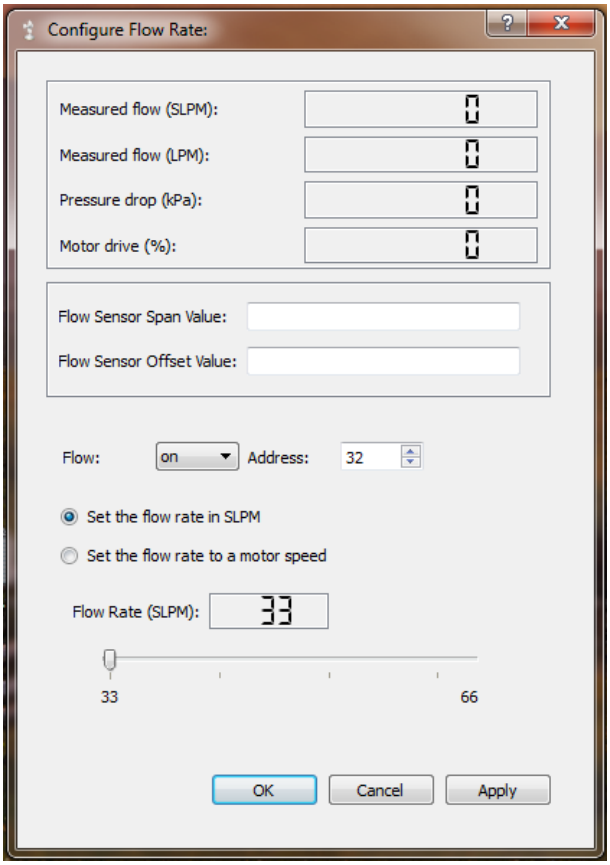


Figure 16: Flow Control Configured for Standard Liters per Minute

The user shall be able to configure the flow control in one of two ways:

- Constant Flow with a range of 33-66 liters per minute (SLPM)
- Constant flow motor speed with a range of 0 – 100%

The figure above indicates that the flow is set for constant flow rate. This dialog will display the present air flow in terms of Standard Liters per Minute (SLPM) and Liters per Minute (LPM).

The conversion between the two follows:

$$LPM = SLPM\frac{(T \times 101.325)}{(273.15 \times P)}$$

Where:

$LPM$ = Liters Per Minute
$SLPM$ = Standard Liters Per Minute
$T$ = Temperature measured at the flow control device
$P$ = Pressure measured at the flow control device

Additionally, it will display the pressure drop within the flow module as well as the percentage of power being applied to the flow motor. The user can manipulate the control slider to change the flow rate value within the allowable limits. If the user would prefer a constant motor speed, the user simply selects the "Set the flow rate to a motor speed" radio button and the dialog will alter as shown in Figure 17.

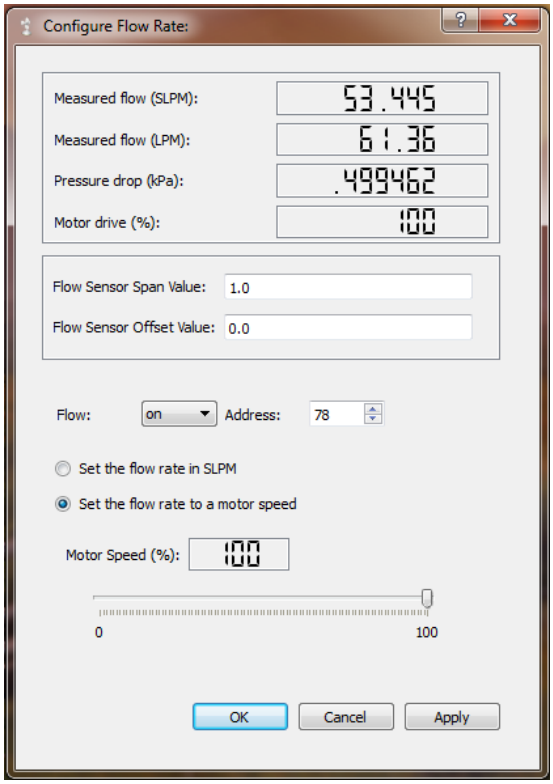


**Figure 17: Flow Control Configured for Constant Motor Speed**

### *4.314 RS-232 Interface*

The instrument will provide two independent RS-232 interfaces. One shall be used as a general purpose output allowing the instrument to send measurement values to an RS-232 based recording device. The other shall serve as a digital input for a sonic anemometer.

To configure the Sonic Anemometer Input RS-232 channel, the user would select the sonic tool bar button (7$^{th}$ from the left with the image of a wind sock, see Figure 10). This will bring up the Sonic configuration dialog as shown in Figure 18.

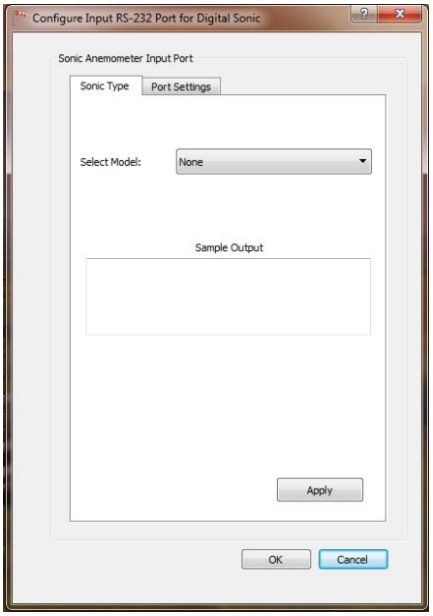


**Figure 18: RS-232 Channel Configured for Sonic Anemometer Input**

As the figure indicates, the channel is configured for input from a sonic anemometer. Given that the serial parameters vary between sonic manufacturers, the user will have full control on how the RS-232 channel can be set up. If the user wishes to use the other RS-232 channel to output the primary data values, the user simply selects the simple DB-9 connector button (8$^{th}$ from the left) and the following configuration dialog will appear as shown Figure 19.

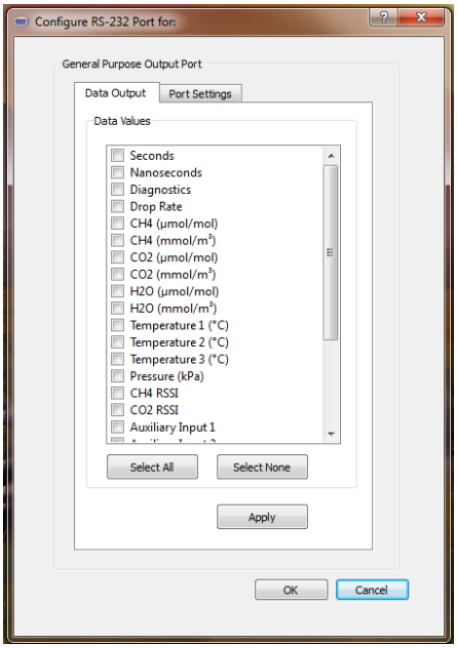


**Figure 19: RS-232 Channel Configured for Primary Data Value Output**

In this dialog, the user has the option of recording all of the RS-232 data or selectively recording certain data values by checking or un-checking the corresponding check boxes.

### *4.315 Logging using the Client Application Computer*

Along with instrument configuration, the client application can also be used to log data from the instrument to the host computer. To do this, the user would press the Configure Logging tool bar button (8th from the left with the image of a floppy disk, see Figure 10). This will bring up the Configure Host PC Logging dialog as shown in Figure 20.

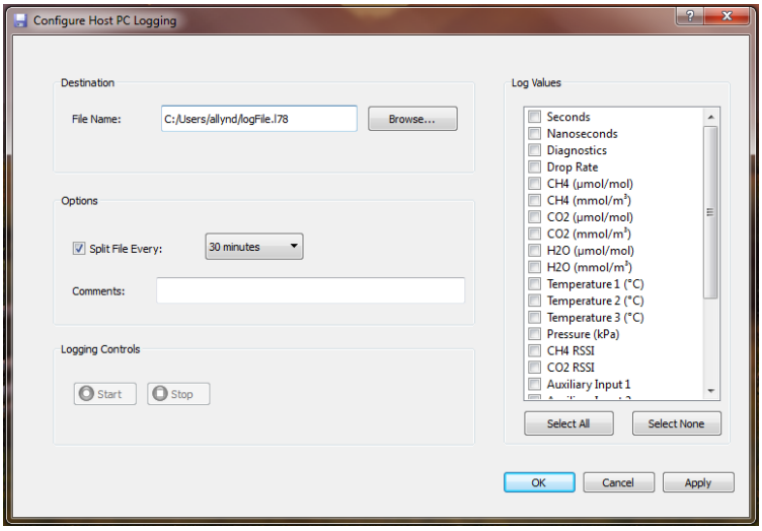


**Figure 20: Configure Host PC Logging Dialog**

Using this dialog, the user will be able to record all or any combination of the primary data values, status values, and diagnostic values. Additionally, the user will be able to have the host PC "split" the log files along the following time intervals:

- every 30 minutes
- every 60 minutes
- every 2 hours
- every 4 hours

Having optional time intervals will address the concern of having excessively large data files and will allow the user to keep them to a more manageable size. Once the configuration is complete, the user simply presses the "Start" button to begin recording. To stop the recording, the user would press the "Stop" button. Pressing the "Start" button again, will append the data to the same file. Otherwise, the user has the option to change the configuration once the recording is stopped.

### *4.316 Web Server*

The instrument shall support a small embedded web server which will enable a user to remotely access the instrument, if it is connected to the internet, using a simple web browser. The embedded web

server will enable a user to alter the instrument's configuration and to determine the status of the instrument. Since the access is through a web browser, the user may use any type of browser device ranging from a standard PC to a smart phone.

As an example, consider the following figure which is the web browser version of the Flow Rate Configuration Dialog:

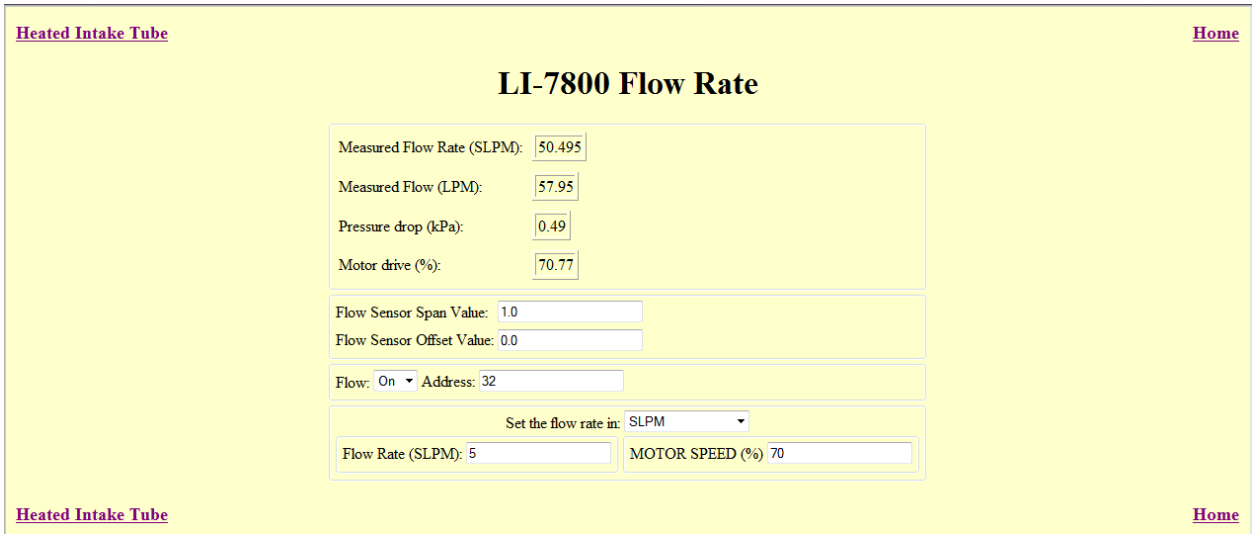


Figure 21: Web Browser Flow Rate Configuration Dialog Box

## 4.32 Communication Protocol

As indicated previously, the client application will connect to the instrument either through an RS-232 connection or a TCP/IP connection. When the connection is made, the application will communicate with the instrument using an eXtensible Mark-up Language (XML) communication protocol of the following form:

```
<licor>
      <li7800>
            <error>{Free form Text}</error>
            <ver>{Version Number}</ver>                    (read-only)
            <serialnumber>{serial number}</serialnumber>(read-only)
            <ipaddress>{current ip address</ipaddress>  (read-only)
            <output>
                  <data>
```

```
            <ch4>{Bool}</ch4>

            <co2>{Bool}</co2>

            <h2o>{Bool}</h2o>

            <temp>{Bool}</temp>

            <press>{Bool}</press>

            <aux1>{Bool}</aux1>

            <aux2>{Bool}</aux2>

            <aux3>{Bool}</aux3>

            <aux4>{Bool}</aux4>

            <enablecrc>{Bool}</enablecrc>

            <rate>{ 0 | 1 | 2 | 5 | 10 | 20 | 30 | 40 | 50
                  }</rate>

      </data>

            …
```

Using the communication protocol in this form allows the user the option of developing a custom communication or recording software client should the installation require it.

## 4.33 Embedded

### *4.331 Field-Programmable Gate Array (FPGA)*

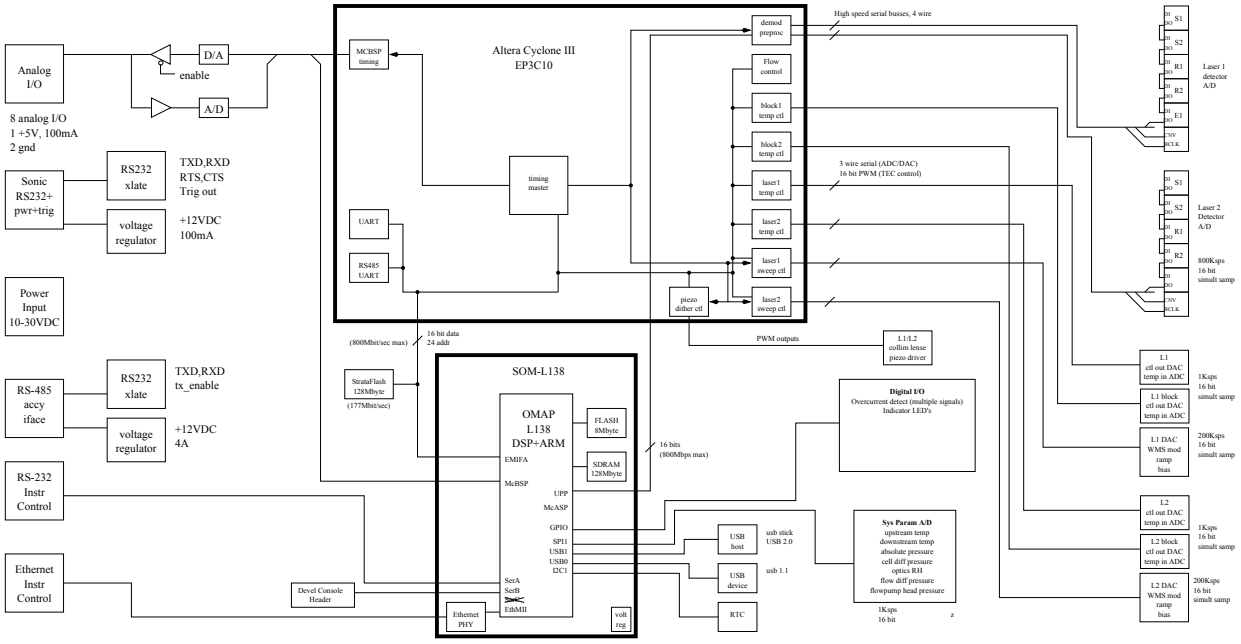


**Figure 22: FPGA/DSP Block Diagram**

The block diagram for the FPGA and DSP subsections is shown in Figure 22. The job of the FPGA has been expanded somewhat from the initial proposal. The additional processing required by the high speed data collection and digital demodulation will be performed inside the FPGA. The processed datasets will be sent to the DSP for fitting operations and final output.

### *4.332 DSP*

The DSP will be responsible for processing the FPGA output into final gas concentration measurements and fit quality measurements. The algorithm used depends on the nature of the measurement. For the $CH_4$ channel, the final processing will consist of a line-lock servo loop and an SVD fitting algorithm to generate an intermediate output. The intermediate output is then processed with temperature and pressure measurements to produce the final concentration measurement. For the $CO_2$ and $H_2O$ channels, a new fitting algorithm is under development to process the direct absorption measurements into $CO_2$ and $H_2O$ concentration measurements.

### *4.333 ARM – Linux Embedded Software Package*

The embedded software application is currently being developed to support an ARM processor with an onboard Digital Signal Processing (DSP) unit. The two processing elements are using a shared memory region to facilitate inter-processor communications and streamline the input and output processing tasks. All data collection, de-modulation, and filtering is being performed on the DSP processor while the network and calibration routines are handled on the ARM.

### *4.334 Algorithms*

Figure 23 through Figure 26 are screenshots from a fully functioning breadboard prototype controlled by a personal computer and Labview. The processing algorithms are the same as intended in the final

FPGA/DSP implementation. Fit vectors are pre-calculated for a given temperature and pressure. The results when measured at 10 Hz proved to have a RMS noise level better than 0.2 ppm for $CO_2$ and 10 ppm for water with an excellent fit to the spectra with low residuals and no crosstalk to the first order. Additional testing in greater detail will be performed with a range of calibration gases and a water vapor generator.

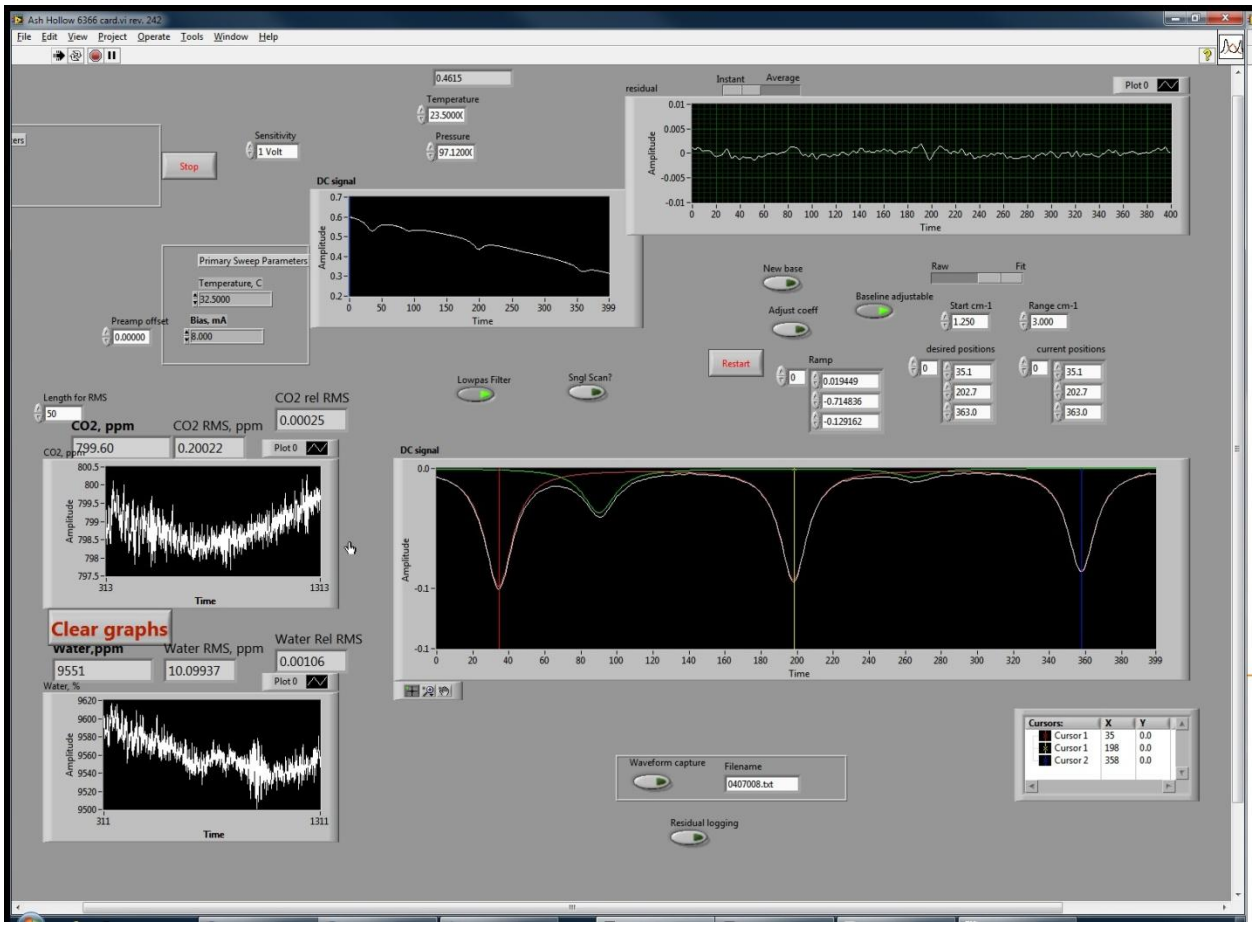


**Figure 23: Front Panel of LabView VI**

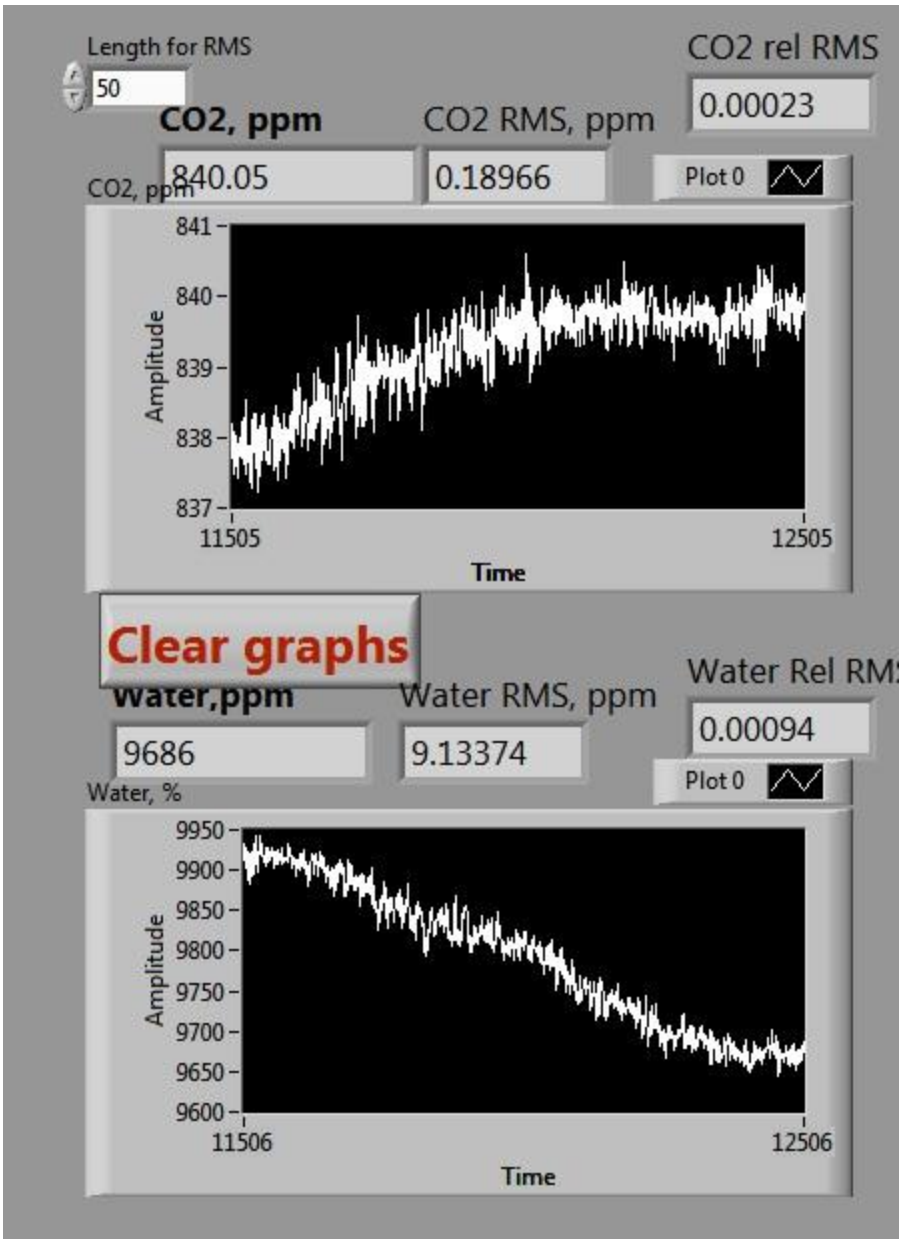


Figure 24: Ambient Air and Short Term RMS Noise Measurements

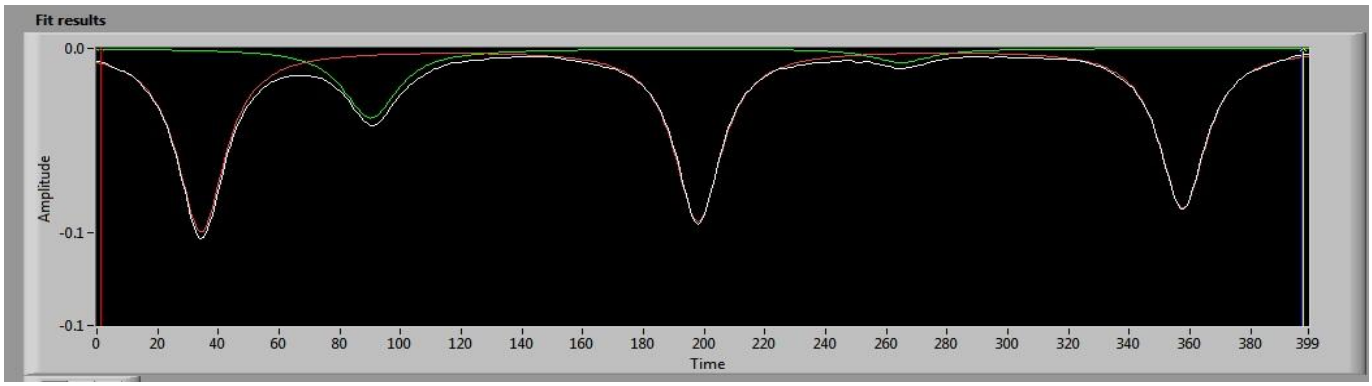


Figure 25: 3cm$^{-1}$ Water Vapor and $CO_2$ Scan of Linear Fit of the Absorbance

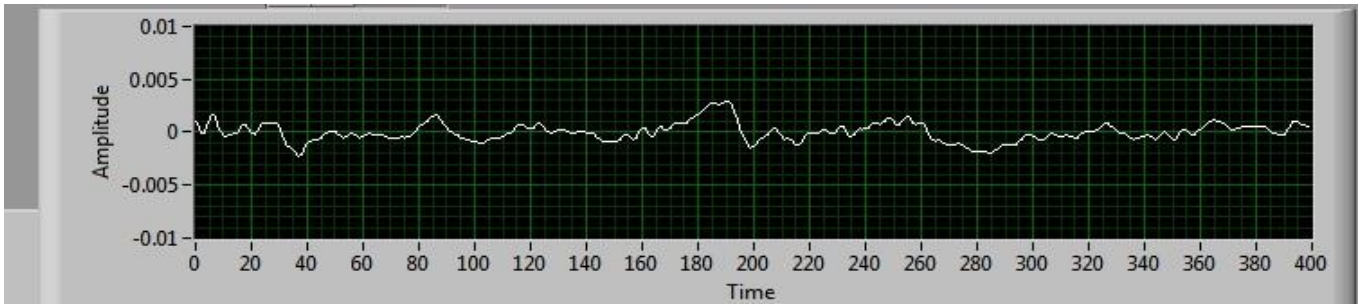


Figure 26: Residual Noise from Figure 25

# 5.0 Prototype Performance from Laboratory Testing

## 5.1 Calibration Accuracy Results

A bench top prototype has been used to determine linearity of the response using a range of $CO_2$ concentrations and a LI-COR LI-610 dew point generator. The response to change in $CO_2$ concentration is linear and shows less than three percent error even without calibration.

Figure 27

Figure 27: $CO_2$ Calibration Plot

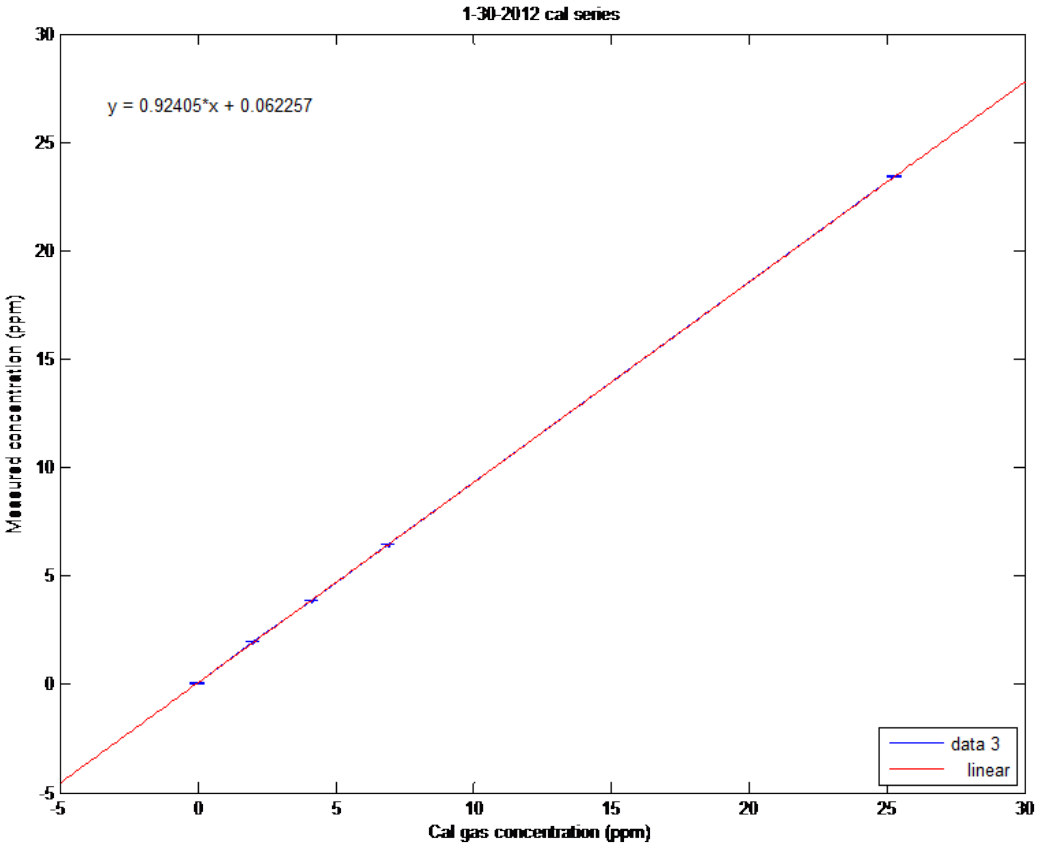


Figure 28: $CH_4$ Calibration Plot

The water signal exhibits a slight non-linearity due to substantial self-broadening (0.416 $cm^{-1}$/atm vs. 0.077 $cm^{-1}$/atm for air broadening). This can be easily corrected using an estimate of water vapor in the calculation of fit vectors prior to the fit or using a quadratic calibration function. Figure 29 shows the linearity of the response after correction for self-broadening by using a second order calibration function.

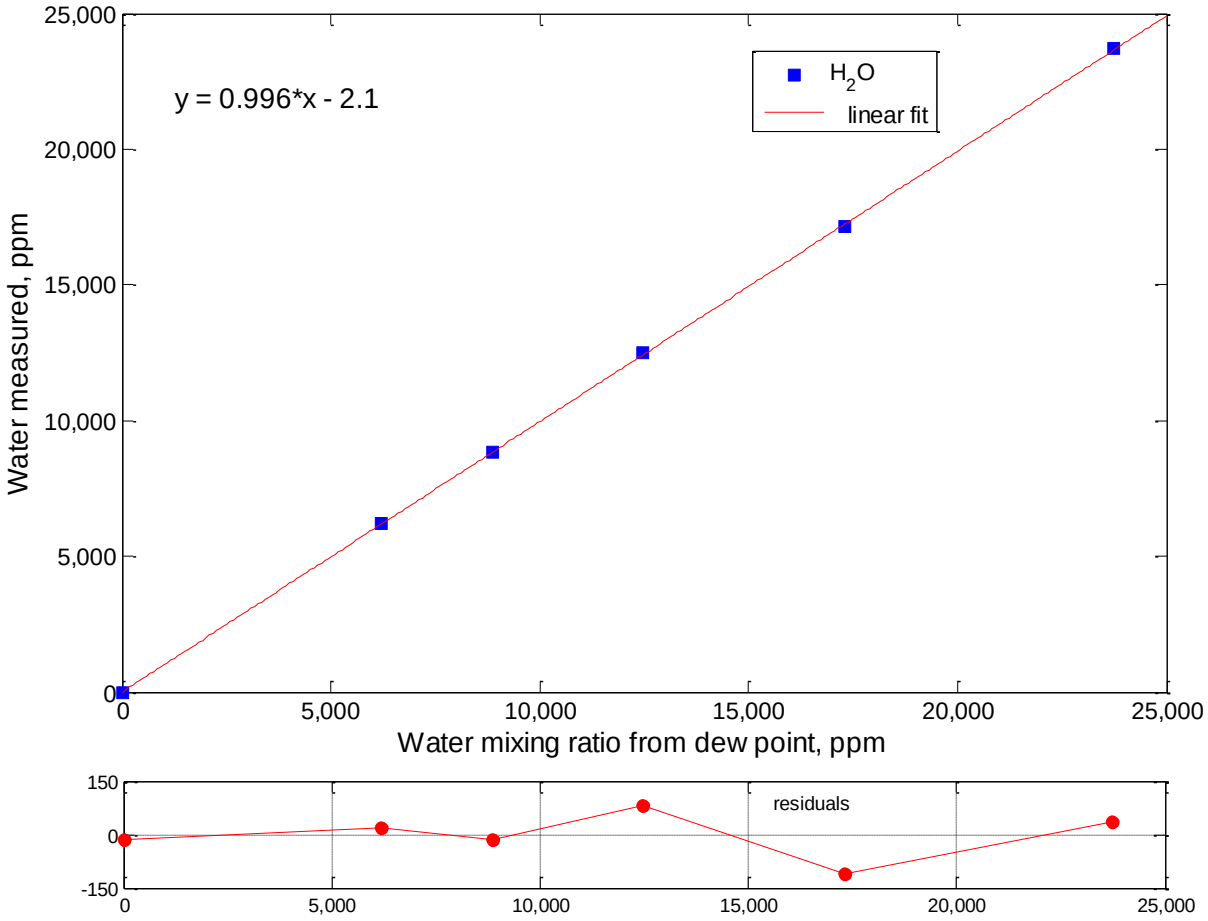


Figure 29: Water Calibration Plot

We also looked at cross talk between $CO_2$ and water. Figure 30 shows a plot of errors in water vapor due to $CO_2$. On the right axis there is an absolute error in water vapor mole fraction (always below 400 ppm), and on the left axis is a corresponding error in calculating a dry mole fraction of $CO_2$. In the range of 0-2,000 ppm $CO_2$ and 5,000-25,000 ppm of water this error is below 0.04 percent.

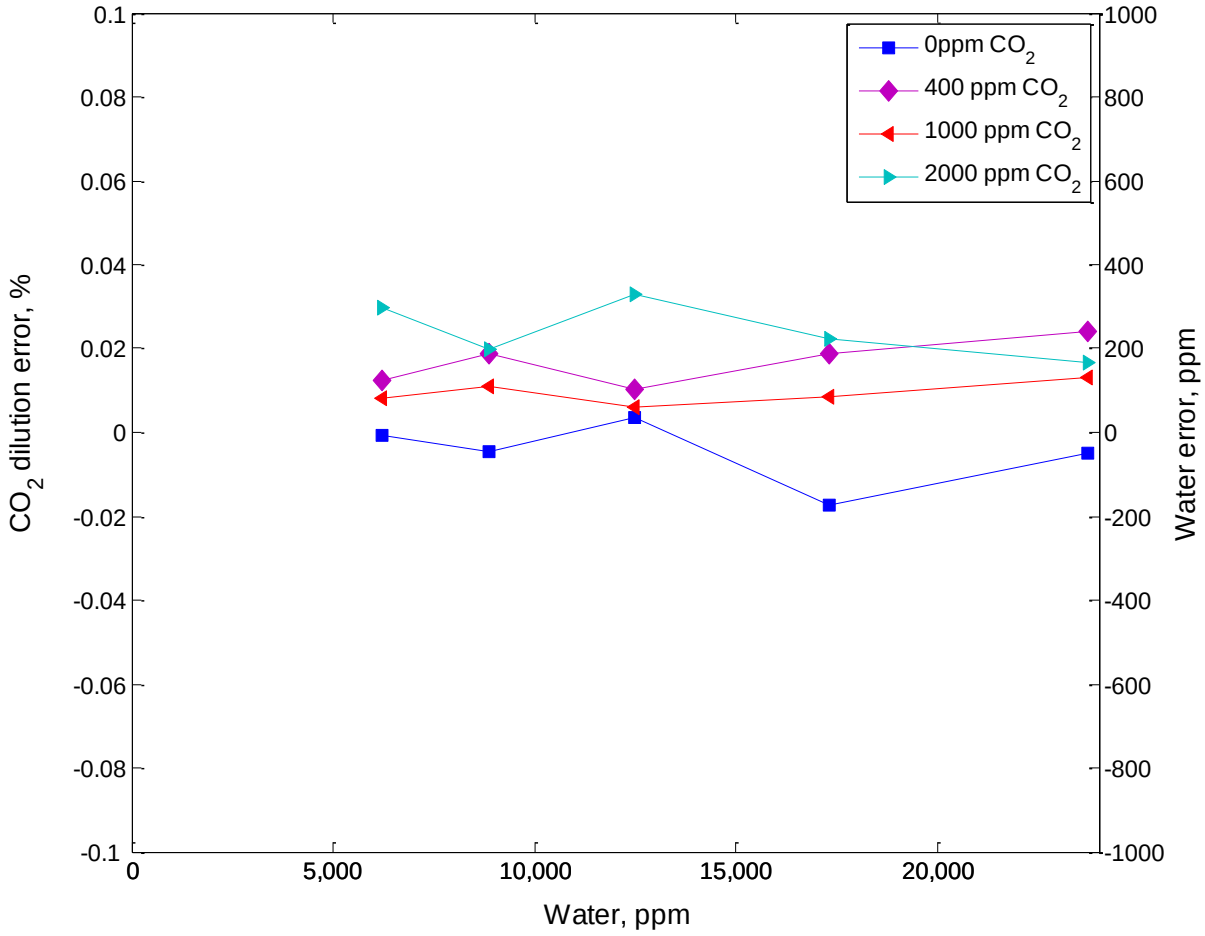


**Figure 30: Cross talk from $CO_2$ on Water Signal**

Figure 31 shows a relative error in $CO_2$ mole fraction as a function of water vapor after the effect of dilution is taken into account. The slopes for different concentration of $CO_2$ are similar which strongly suggests that this is due to additional broadening of $CO_2$ lines by water vapor, and it requires more careful study. This error can also be easily corrected either by using an estimate for water vapor prior to the fit or using an additional multiplier on the dilution factor in dry mole fraction calculation.

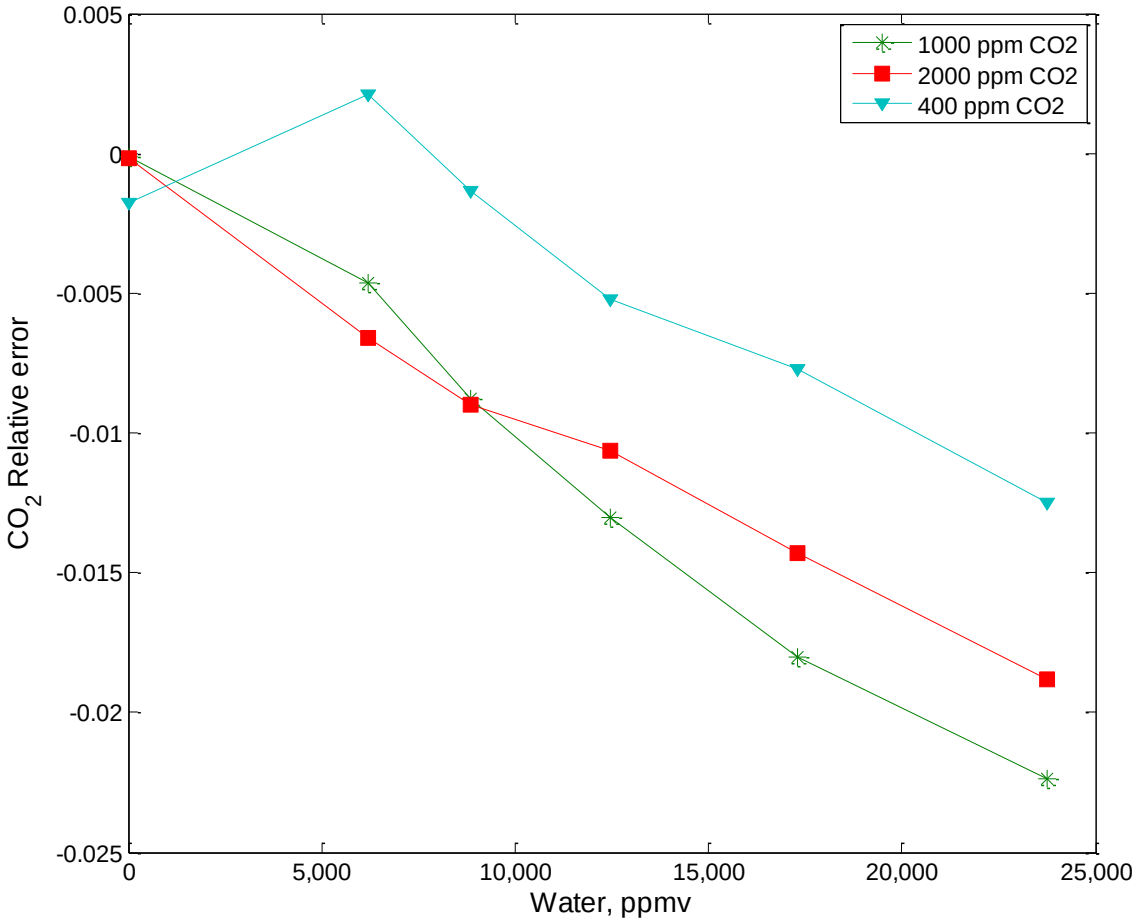


Figure 31: Crosstalk from $H_20$ on $CO_2$ Signal with Dilution Factored

## 5.2 RMS Noise at Various Sampling Rates

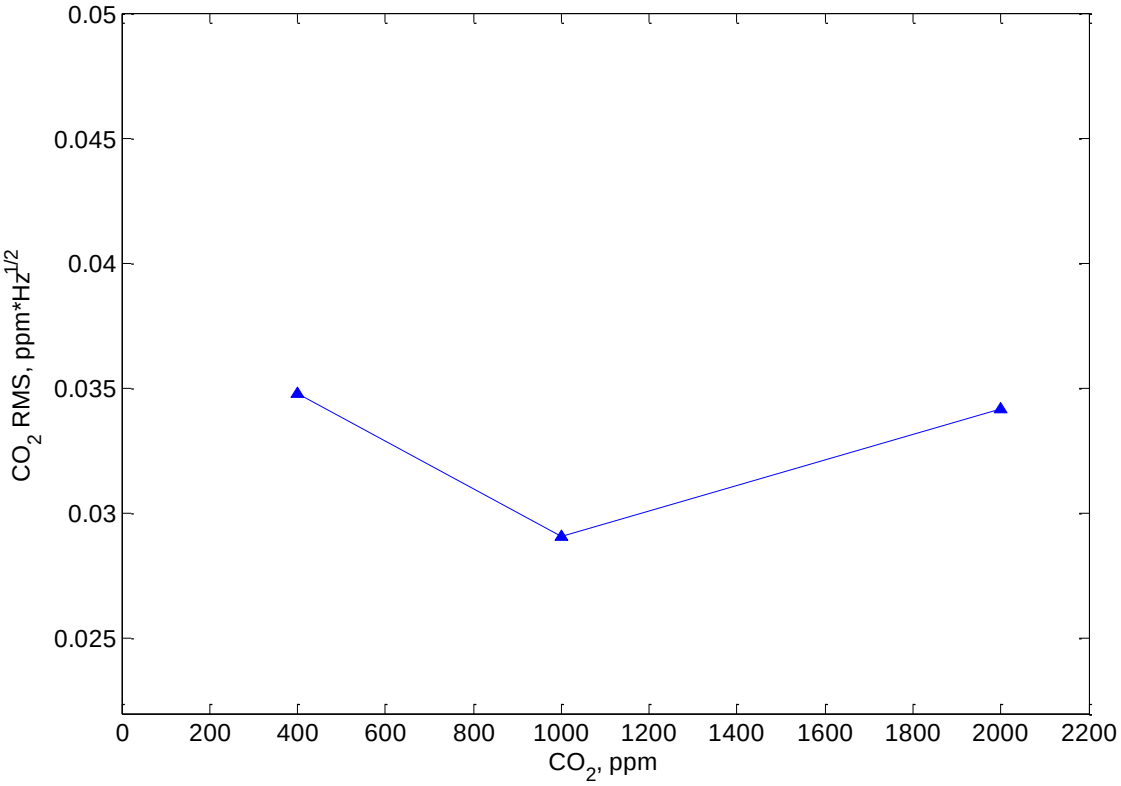


Figure 32: RMS for $CO_2$

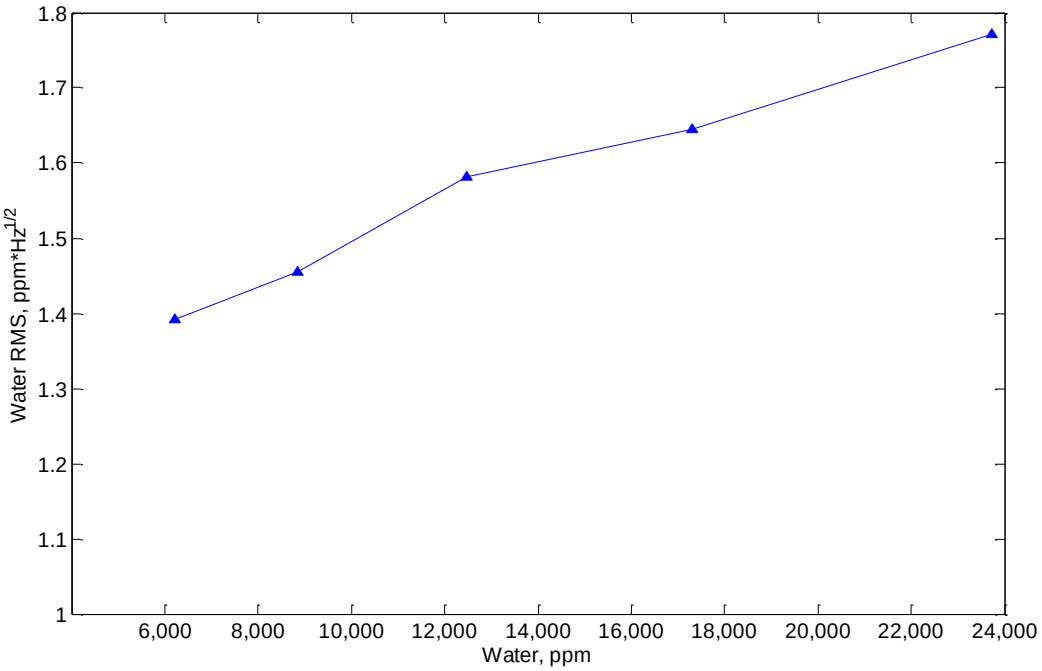


**Figure 33: RMS for Water**

In Figure 34 below, the calibration gas used is plotted on the x-axis versus the measured quantity from the prototype bench. Accuracy of the calibration gas is ± one percent. Rigorous calibrations were not done in advance; therefore, the slope and offset of the linear fit differ from one and zero respectively. Approximately one minute of 1Hz data was collected for each point. Error bars on Figure 34 represent 1-sigma for approximately one minute of data. The residuals in the plot below the calibration series are the deviation of the data from the fitted line. The laser used for collecting this data did not have wavelength feedback control but was controlled using a fixed temperature. The implications of using a fixed temperature control rather than active feedback is larger long term temperature drift, higher resolution numbers, and less accuracy.

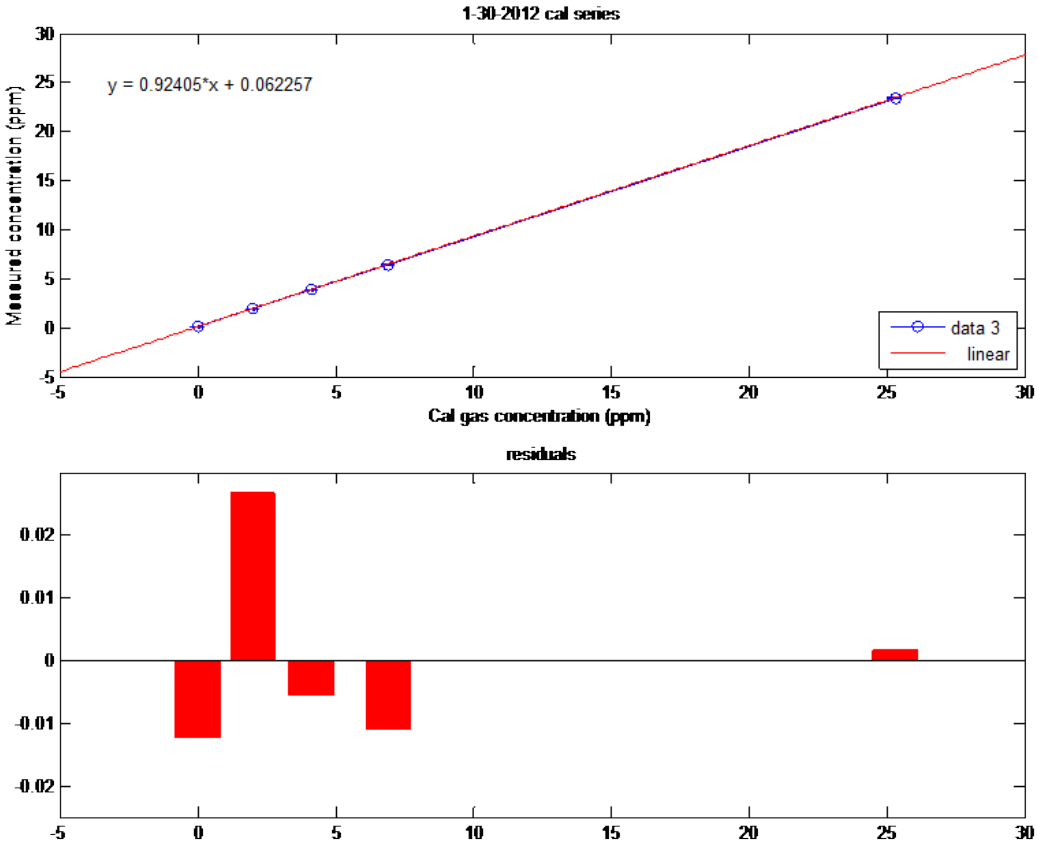


Figure 34: Calibration Gas vs. Measured Concentration

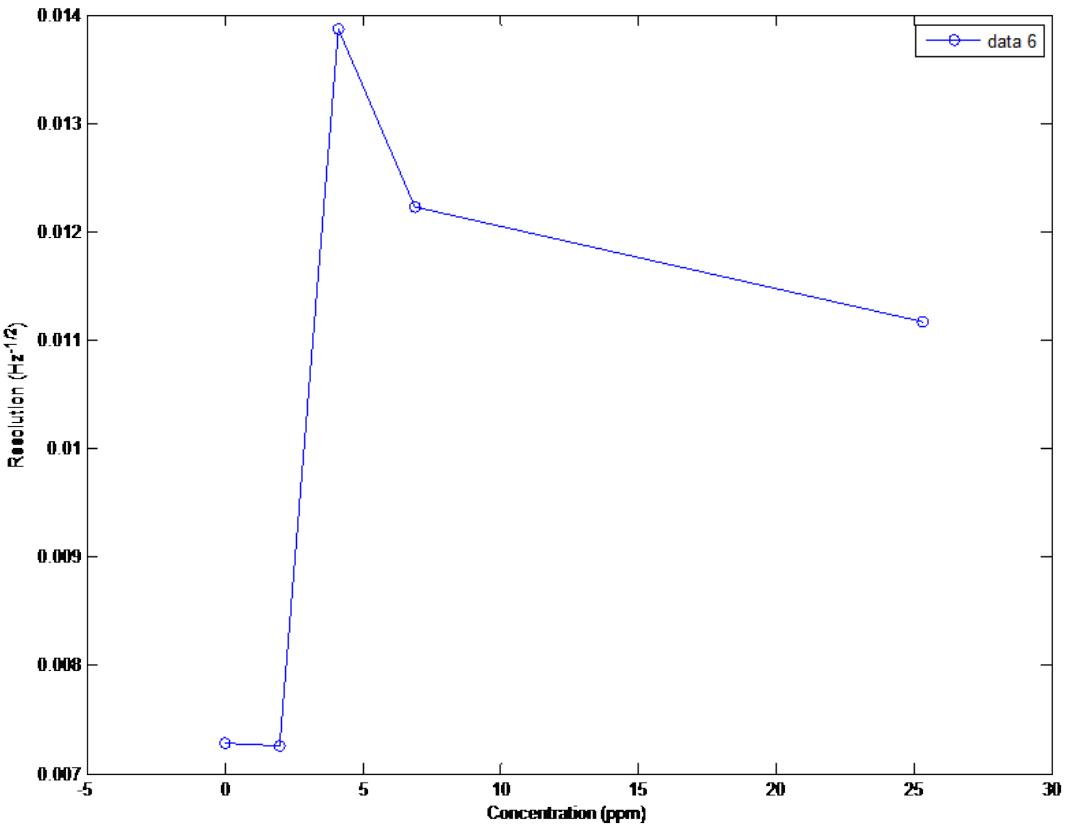


Figure 35: Plot of Error Bar Amplitude from Figure 34.

The data points in Figure 35 represent 1-sigma of approximately 60 data points. These numbers are expected to be lower with the implementation of active temperature tuning for wavelength control.

## 6.0 References

Andrews AE, Bruhwiler L, Crotwell A, Dlugokencky EJ, Hahn MP, Hirsch AI, Kitzis DR, Lang PM, Masarie KA, Michalak AM, Miller JB, Novelli PC, Peters W, Tans PP, Thoning KW, Vaughn1 BH, Zhao C. 2004. Carbon cycle greenhouse gases. In: Conway TJ [ed.] *Climate monitoring and diagnostics laboratory, summary report # 27* (2002-2003). pp 32-57.

Billesbach DP, Kim J, Clement RJ, Verma SB, Ullman FG. 1998. An inter-comparison of two tunable diode laser spectrometers used for eddy correlation measurement of methane flux in a prairie wetland. *Journal of Atmospheric and Oceanic Technology*. **15**: 197-206.

Bousquet P, Ciais P, Miller JB, Dlugokencky EJ, Hauglustaine DA, Prigent C, Van der Werf GR, Peylin P, Brunke EG, Carouge C, Langenfelds RL, Lathiere J, Papa F, Ramonet M, Schmidt M, Steele LP, Tyler SC, White J. 2006. Contribution of anthropogenic and natural sources to atmospheric methane variability. *Nature.* **443**: 439–443.

Cunnold DM, Steele LP, Fraser PJ, Simmonds PG, Prinn RG, Weiss RF, Porter LW, O'Doherty S, Langenfelds RL, Krummel PB, Wang HJ, Emmons L, Tie XX, Dlugokencky EJ. 2002. In situ measurements of atmospheric methane at GAGE/AGAGE sites during 1985-2000 and resulting source inferences. *Journal of Geophysical Research,* **107***:* doi:10.1029/2001JD001226.

Dengel S, Levy, PE, Grace J, Jones SK, and Skiba UM. 2011. Methane emissions from sheep pasture, measured with an open-path eddy covariance system. *Global Change Biology*, 17:3524-3533. doi: 10.1111/j.1365-2486.2011.02466.x

Detto M, Verfaillie J, Anderson F, Xu L, Baldocchi DD, 2011. Comparing laser-based open-and closed-path gas analyzers to measure methane fluxes using the eddy covariance method. *Agricultural and Forest Meteorology*. , doi: 10.1016/j.agrformet.2011.05.014

Dlugokencky EJ, Masarie KA, Lang PM, Tans PP. 1998. Continuing decline in the growth rate of atmospheric methane. *Nature.* **393**:447–450.

Dlugokencky EJ, Houweling S, Bruhwiler L, Masarie KA, Lang JB, Tans PP. 2003. Atmospheric methane levels off: Temporary pause or a new steady-state? *Geophysical Research Letters*. **30**: doi:1029/2003GL018126.

Dlugokencky, EJ, Myers RC, Lang PM, Masarie KA, Crotwell AM, Thoning KW, Hall BD, Elkins JW, Steele LP. 2005. Conversion of NOAA CMDL atmospheric dry air $CH_4$ mole fractions to a gravimetrically prepared standard scale. *Journal of Geophysical Research*, **110:** D18306, doi:10.1029/2005JD006035.

Dueck TA, de Visser R, Poorter H, Persijn S, Gorissen A, de Visser W, Schapendonk A, Verhagen J, Snel J, Harren FJM, Ngai AKY, Verstappen F, Bouwmeester H, Voesenek LACJ, van der Werf A. 2007. No evidence for substantial aerobic methane emission by terrestrial plants: $\delta^{13}$C-labelling approach. *New Phytologist.* **175:** 29–35.

Ehhalt D, Prather M. 2001. Chapter 4. Atmospheric chemistry and greenhouse gases. In: Houghton, JT., et al., (Eds.). Climate Change 2001: The Scientific Basis, Contribution of Working Group I to the

Third Assessment Report of the Intergovernmental Panel on Climate Change. Cambridge University Press, Cambridge, UK.

Etheridge DM, Steele LP, Francey RJ, Langenfelds RL. 1998. Atmospheric methane between 1000 A.D. and present: Evidence of anthropogenic emissions and climatic variability. *Journal of Geophysical Research.* **103:** 15979–15993.

Evans J.R. 2007. Resolving methane fluxes. *New Phytologist*. **175:** 1-4.

Fung IJ, Lerner JJ, Matthews E, Prather M, Steele LP, Fraser PJ. 1991. Three-dimensional model synthesis of the global methane cycle. *Journal of Geophysical Research.* **96**: 13033-13065.

Hansen JE, and Sato M. 2001. Trends of measured climate forcing agents. *Proceedings of the National Academy of Sciences of the United States of America*. **98**: 14778-14783.

Hendriks DMD, Dolman AJ, van der Molen MK, van Huissteden J. 2008. A compact and stable eddy covariance set-up for methane measurements using off-axis integrated cavity output spectroscopy. *Atmospheric Chemistry and Physics*. **8**: 431-443.

Houweling S, Kaminski T, Dentener F, Lelieveld J, Heimann M. 1999. Inverse modeling of methane sources and sinks using the adjoint of a global transport model. *Journal of Geophysical Research.* **104:** 26137-26160.

IPCC, 2007**.** Contribution of Working Group I to the Fourth Assessment Report of the Inter-governmental Panel on Climate Change, Summary for Policymakers.

Keppler F, Hamilton JTG, Brad M, Röckmann T. 2006. Methane emissions from terrestrial plants under aerobic conditions. *Nature.* **439:** doi:10.1038/nature04420.

Kim J, Verma SB, Billesbach DP, Clement RJ. 1998. Diel variation in methane emission from a midlatitude prairie wetland: Significance of convective throughflow in Phragmites australis. *Journal of Geophysical Research*. **103**: 8029-28039.

Kroon PS, Hensen A, Jonker HJJ, Zahniser MS, van't Veen WH, Vermeulen AT., 2007. Suitability of quantum cascade laser spectroscopy for $CH_4$ and $N_2O$ eddy covariance flux measurements. *Biogeosciences.* **4:** 715-728.

Lelieveld J, Crutzen P, Dentener J. 1998. Changing concentration, lifetime and climate forcing of atmospheric methane. *Tellus B*. **50**: 128-150.

McDermitt D, Burba G, Xu L, Anderson T, Komissarov A, Riensche B, Schedlbauer J, Starr G, Zona D, Oechel W, Oberbauer S, Hastings S. 2011. A new low-power, open-path instrument for measuring methane flux by eddy covariance. *Applied Physics B: Lasers and Optics*, **102**, 391-405.

McManus JB, Nelson DD, Shorter JH, Zahniser MS. 2002. Quantum cascade lasers for open-and closed-path measurement of atmospheric trace gases, *Diode Lasers and Application in Atmospheric Sensing, SPIE Proceedings.* **4817**: 22-33.

McManus JB, Zahniser MS, Nelson DD, Williams LR, Kolb CE. 2002. Infrared laser spectrometer with balanced absorption for measurement of isotopic ratios of carbon gases. *Spectrochimica Acta*. **58**: 2465-2479.

Nelson DD, McManus JB, Urbanski S, Herndon S, Zahniser MS. 2004. High precision measurements of atmospheric nitrous oxide and methane using thermoelectrically cooled mid-infrared quantum cascade lasers and detectors. *Spectrochimica Acta.* **60**: 3325-3335.

Nisbet RER, Fisher R, Nimmo RH, Bendall DS, Crill PM, Gallego AV, Hornibrook ERC, López-Juez E, Lowry D, Nisbet PBR, Shuckburgh EF, Sriskantharajah S, How CJ, Nisbet EG. 2009. Emission of methane from plants. *Proceedings of Royal Society London, Ser. B.* **276:**1347-1354.

Rigby M, Prinn RG, Fraser PJ, Simmonds PG, Langenfelds RL, Huang J, Cunnold DM, Steele LP, Krummel PB, Weiss RF, O'Doherty S, Salameh PK, Wang HJ, Harth CM, Mühle J, Porter LW. 2008. Renewed growth of atmospheric methane. *Geophysical Research Letter*. **35:** doi:10.1029/2008GL036037.

Rohde H. 1990. A comparison of the contribution of various gases to the greenhouse effect. *Science.* **248**: 1217-1219.

Simpson IJ, Blake DR, Rowland FS, Chen TY. 2002. Implications of the recent fluctuations in the growth rate of tropospheric methane. *Geophysical Research Letter*, **29**(10): doi:10.1029/2001GL014521.

Von Fisher JC, Hedin LO. 2007. Controls on soil methane fluxes: Tests of biophysical mechanisms using stable isotope tracers. *Global biogeochemical Cycles*. **21**: doi: 10.1029/2006GB002687.

Vourlitis GL, Oechel WC, Hastings SJ, Jenkins MA. 1993. The effect of soil moisture and thaw depth on $CH_4$ flux from wet coastal tundra ecosystems on the north slope of Alaska. *Chemosphere*. **26**: 329-337.